Spring 2012

Maximum power point tracking control of hydrokinetic turbine and low-speed high-thrust permanent magnet generator design

Hailong Zhou

Department:

MAXIMUM POWER POINT TRACKING CONTROL OF HYDROKINETIC TURBINE AND LOW-SPEED HIGH-THRUST PERMANENT MAGNET GENERATOR DESIGN

by

HAILONG ZHOU

A THESIS

Presented to the Faculty of the Graduate School of the

MISSOURI UNIVERSITY OF SCIENCE AND TECHNOLOGY

In Partial Fulfillment of the Requirements for the Degree

MASTER OF SCIENCE IN ELECTRICAL ENGINEERING

2012

Approved by

Jonathan W. Kimball, Advisor
Keith Corzine
Mehdi Ferdowsi

ABSTRACT

River-based hydrokinetic turbine power generation systems have been studied to introduce an effective energy flow control method. Hydrokinetic turbine systems share a lot of similarities with wind turbine systems in terms of physical principles of operation, electrical hardware, and variable speed capability for optimal energy extraction. A multi-pole permanent magnet synchronous generator is used to generate electric power because of its ability to reach high power density and high thrust at low speed. A 3-phase diode rectifier is used to convert AC power from the generator into DC power and a boost converter is used to implement energy flow control. On the load side, an electronic voltage load is used for test purposes to simulate a constant DC bus voltage load, such as a battery. A dynamic model of the entire system is developed and used to analyze the interaction between the mechanical structure of water turbine and electrical load of the system, based on which a maximum power point tracking control algorithm is developed and implemented in the boost converter. Simulation and experimental results are presented to validate the proposed MPPT control strategy for hydrokinetic turbine system. Similar to the wind turbine system, hydrokinetic turbine system usually requires a gear box to couple the turbine and the generator because the operating speed range for the hydrokinetic turbine is much lower than the operating speed range for most PMSGs. However, the gear box coupling adds additional transmission power losses. Therefore a high-thrust low-speed permanent magnet synchronous generator is designed to couple with the water turbine without a gear box.

ACKNOWLEDGMENTS

I would like to thank my advisor Dr. Jonathan Kimball for his direction, guidance and encouragement throughout my Master's program. Dr. Kimball's has given me great help with my research and his vast knowledge in the electrical engineering field has always been a motivation to me as an electrical engineering student. Dr. Kimball's vision and interest in the renewable energy field and power electronic devices' application in renewable energy systems has made my research possible and for that I would like to express my deepest gratitude.

I would also like to thank the members of my committee, Dr. Keith Corzine and Dr. Mehdi Ferdowsi for their interest in my research topic and their continuous support through my graduate studies. Their instructions on electric drive systems and advanced power electronics have also benefited me significantly.

Special thanks to Mr. Peter D. Stueber who has always encouraged and helped me in my life whenever I am confused and lost. It was his continuous support that kept me motivated.

I would especially like to thank my parents and my family members for their tremendous support throughout my studies. My parents have sacrificed a lot for me and for that I am grateful from the bottom of my heart.

Finally, I would like to gratefully acknowledge the support of the Office of Naval Research through contract ONR N000141010923 (Program Manager- Dr. Michele Anderson). It is their financial support that has made my research possible.

TABLE OF CONTENTS

LIST OF ILLUSTRATIONS

Page

LIST OF TABLES

Page

NOMENCLATURE

Symbol	Description
HTECS	Hydrokinetic Turbine Energy Conversion System
WTECS	Wind Turbine Energy Conversion System
MPPT	Maximum Power Point Tracking
PMSG	Permanent Magnet Synchronous Generator
HTS	Hydrokinetic Turbine System
DFIG	Doubly-Fed Induction Generator
P_m	Turbine Output Power
ρ	Water Density
r	Blade Radius
λ	Tip Speed Ratio
β	Pitch Angle
v	Water Speed
ω_m	Turbine Rotational Speed
C_p	Power Coefficient
B	Number of Blades
C_l	Lift Coefficient
C_d	Drag Coefficient
E	Back EMF
R	Phase Resistance
L	Phase Inductance of The PMSG
K	Back EMF Constant
ω_e	Electrical Frequency
I	Phase Current
V_d	Rectifier Output Voltage
V_{LL_peak}	Line to Line Peak Voltage of the PMSG
V_{LL}	Line to Line RMS Voltage of The PMSG
V	Phase Voltage
I_d	Rectifier Output Current

P_g	Generator Output Power
D	Duty Ratio
V_{bus}	DC Bus Voltage
B_g	Air Gap Flux Density
α_m	Manget Fraction
C_Φ	Flux Concentration Factor
P_c	Permeance Coefficient
k_{ml}	Leakage Factor
k_c	Carter coefficient
B_r	Remanence
E_{max}	Max Back EMF

1. INTRODUCTION

1.1. MOTIVATION

As a result of rising concerns over greenhouse gas emissions, the environment, rising electricity demand and exhaustion of fossil energy sources, trends in energy production have become more and more focused on using renewable energy resources such as wind, solar, hydro, biomass and geothermal [1-3]. Among these renewable energy resources, hydro and wind power have great potentials of development to be able to compete with the classical fossil energy sources such as coal, oil and natural gas [4]. Wind power over the past decade, has undergone a substantial advancement in terms of control strategies, custom designed generators, maintenance cost and cost competitiveness, becoming more and more important in renewable energy market [5]. Hydroelectricity has been utilized all over the world for decades, usually in the form of high power hydroelectric stations which require the construction of impoundments or diversion of conventional hydroelectric facilities based on dams or penstocks. Nowadays, since the suitable sites for these plants are rare and concerns over the effects of these plants on local environment rise, it is no more possible to set up such plants in most European and North-American countries. Nonetheless substantial capacities of these hydroelectricity plants remain in Africa, Asia, and South America [6]. In order to utilize the vast potential of hydro energies without the construction of dams and penstocks, hydrokinetic turbine energy conversion system (HTECS) becomes more and more popular and is at the forefront of pre-commercial or commercial deployment at various locations in the world [7].

Hydrokinetic turbines share many similarities with wind turbines in terms of physical principles of operation, electrical hardware, and variable speed capability for optimal energy extraction [8]. Therefore, HTECS can benefit in many ways from the many years of advanced development in the wind turbine energy conversion system (WTECS). However, significant differences between HTECS and WTECS do exist, such as a narrower tip speed ratio range, cavitation limits and the requirement to deal with harsh environments for HTECS [9]. One of the most significant differences between WTECS and HETCS is that wind speed varies dramatically over timescales of seconds to

minutes while water speed tends to be relatively constant with seasonal variations. Since the maximum output power point for the same wind turbine varies under different wind speeds, the maximum power point tracking (MPPT) control for wind turbines has been the subject of detailed research [10-12]. Though water speed tends to be relatively constant with small seasonal variations, the fact that water density is more than 800 times bigger than air density means that even a small water speed variation would yield a substantial output power change. Therefore, a maximum power point tracking strategy for the hydrokinetic turbine system is necessary to be able to extract the maximum amount of potential power from the hydrokinetic turbine.

In order to convert the mechanical hydrokinetic energy into electrical power, electrical generators, such as permanent magnet, synchronous and induction generators, are used. For small scale HTECS and WTECS, permanent magnet synchronous generators (PMSG) are widely used because of their high reliability, simple structure, low noise and high power density [13]. Then the electrical power is processed using power electronic devices such as ac-dc rectifier (controlled/uncontrolled), dc-dc converter and dc-ac inverter [14]. Based on whether the system is interfaced with grid or not, hydrokinetic turbine systems, like wind turbine systems, have two types of configurations in general. One is grid-tie hydrokinetic turbine system and the other one is stand-alone hydrokinetic turbine system as shown in Fig. 1.1 and Fig. 1.2 respectively. For grid-tie hydrokinetic turbine systems, a dc-ac inverter is necessary to convert dc power into ac power to interface with the grid. For stand-alone hydrokinetic turbine systems, battery banks are usually used to store the extracted energy as well as to provide a constant dc bus voltage on the load side. DC battery bank can store extra energy when the load power demand is less than the available power from the hydrokinetic turbine and output power when the load power demand exceeds the available power from the hydrokinetic turbine [13, 15]. Stand-alone hydrokinetic systems are common in rural areas where there are no accesses to a power grid [13].

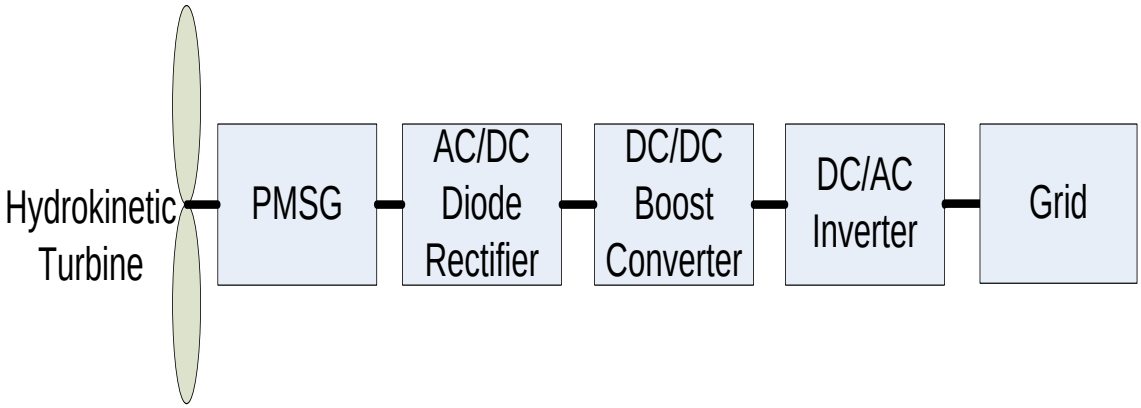

Figure 1.1. Grid-tie hydrokinetic turbine system

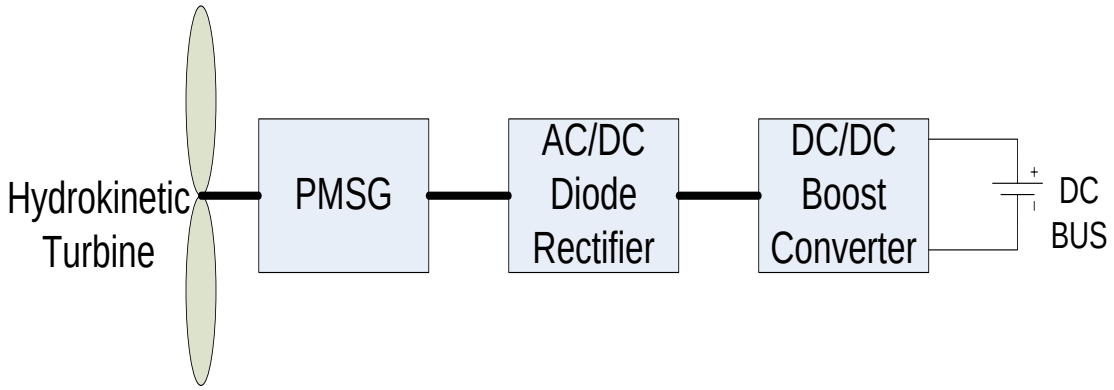

Figure 1.2. Stand-alone hydrokinetic turbine system

1.2. PROPOSED CONTROL APPROACH

Generally, the objective of controlling a turbine system is to maximize the energy yield because with different water (or wind) velocity, the maximum power point for the hydrokinetic (or wind) turbine occurs at different turbine rotor speed [16]. In medium and large turbine systems, pitch angle control is usually adopted to optimize output power as well as to reduce torque and output power variations for high water (or wind) speed [17]. However, for small size turbine systems, the mechanical structure limits make pitch angle control unrealistic [13]. Therefore, a power converter is usually adopted to implement the MPPT control in small-scale turbine systems, such as boost converter. In order to control the operation of the power converter, a microcontroller is needed.

Conventionally, in order for the turbine to operate at maximum power point, the turbine power versus rotational speed characteristic for a specific turbine is stored in a memory. By measuring the rotational speed of the turbine, the difference between the maximum power available and the actually output power can be found. This error between the two power values then feeds back to the control of the generator so that it can operate at the speed that will generate maximum power [13]. However, pre-measuring the turbine power versus speed characteristic is costly for small-scale turbine systems. Therefore, a dynamic MPPT control strategy for a small-scale hydrokinetic turbine system is proposed in this thesis. This proposed MPPT control approach enables the system to dynamically track the maximum power point of the hydrokinetic turbine without pre-measuring the power versus rotational speed characteristics of the hydrokinetic turbine. Figure 1.3 shows the system configuration of the stand-alone hydrokinetic turbine system with the proposed MPPT control implemented in a boost converter.

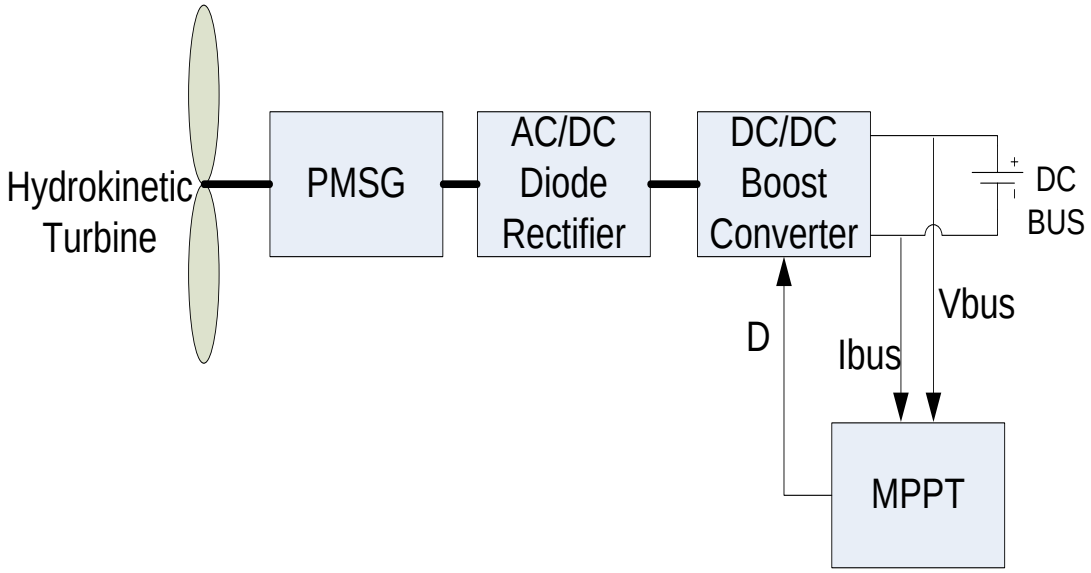

Figure 1.3. Stand-alone hydrokinetic turbine system with MPPT control implemented in the boost converter

In this control method, the output voltage and current are constantly measured and updated by the microcontroller, which would give the value of the output power. Based on the change of the output power, the duty ratio will be changed accordingly. Since the output voltage is constant, varying the duty ratio of the boost converter will cause the output voltage of the rectifier to change which, as a result, will change the rotational speed of the generator.

1.3. DOCUMENT ORGANIZATION

This thesis is organized into four sections. Section 1 provides a general introduction for the hydrokinetic system and a proposed MPPT control approach for hydrokinetic turbines.

Section 2 describes the system level design of hydrokinetic energy conversion systems. It covers different methods and system configurations for hydrokinetic energy conversion systems such as vertical and horizontal turbine systems, ducted and unducted turbine systems as well as vortex induced vibration systems.

Section 3 presents a dynamic model of the hydrokinetic turbine system based on which a MPPT control method is developed. Simulation in Matlab[1] and experimental results are also presented in this section to validate the proposed control method

Section 4 describes a high-thrust low-speed permanent magnet synchronous generator design for the hydrokinetic turbine systems

Section 5 presents the conclusions. Future work and project extensions for the hydrokinetic system are also discussed in this section

Appendix A contains the schematic and board layout for the 3 phase rectifier and boost converter used for the experiment data collection.

Appendix B contains the C codes of the developed MPPT algorithm implemented in the microcontroller.

---

[1] Matlab is a registered trademark of The MathWorks, Inc.

2. SYSTEM LEVEL DESIGN OF HYDROKINETIC TURBINE SYSTEMS

2.1. HYDROKINETIC ENERGY UTILIZATION

Hydrokinetic energy generation technologies have been under development for decades, but this development has been sporadic and inconsistent. Traditionally, hydrokinetic energy can be categorized as wave energy and current energy such as tidal current, open-ocean current and river current. Wave energy technologies are mostly used in marine hydrokinetic systems. Wave energy converters that are currently under deployment can be categorized as absorbers, attenuators, oscillating water columns, overtopping devices, and inverted pendulums [18]. Hydrokinetic current energy, which is common in both oceans and rivers, is usually converted into electrical energy by hydrokinetic turbines just like the wind kinetic energy is converted into electrical energy by wind turbines. In addition, hydrokinetic current energy can be converted into electrical energy by Vortex Induced Vibration (VIV) systems, in which a cylinder that is submerged into the water would vibrate as the water flow hits the cylinder and this vibration motion is converted into electricity by a linear generator.

2.2. HYDROKINETIC TURBINE SYSTEM DESIGN

2.2.1. Horizontal and Vertical Hydrokinetic Turbine System. The first step to design a hydrokinetic turbine system (HTS) is to decide whether to use horizontal turbine system or vertical turbine system. For vertical hydrokinetic turbine system, the biggest advantage is that it can have its gearbox and generator above water level. However, based on the experiments conducted in [19], the fact that vertical hydrokinetic turbine system can have its gearbox and generator above water level does not seem to have any advantages over the horizontal hydrokinetic turbine because the gearbox and generator in the vertical turbine system would have to be as watertight as the horizontal turbine system. For horizontal hydrokinetic turbine system, the biggest advantage is that it is a conventional turbine system and its characteristics have been studied for decades especially in the wind power industry. In addition, it is easier for horizontal turbine systems to integrate a water speed increaser to increase the water velocity interacting with the turbine blades whereas for vertical hydrokinetic turbine systems, the water

velocity increase may have to be directed at a proper angle based on the turbine blade design to improve the power output [19]. Figure 2.1 shows a ducted horizontal hydrokinetic turbine. With the help of duction to increase the water velocity, the need for a gearbox might be eliminated.

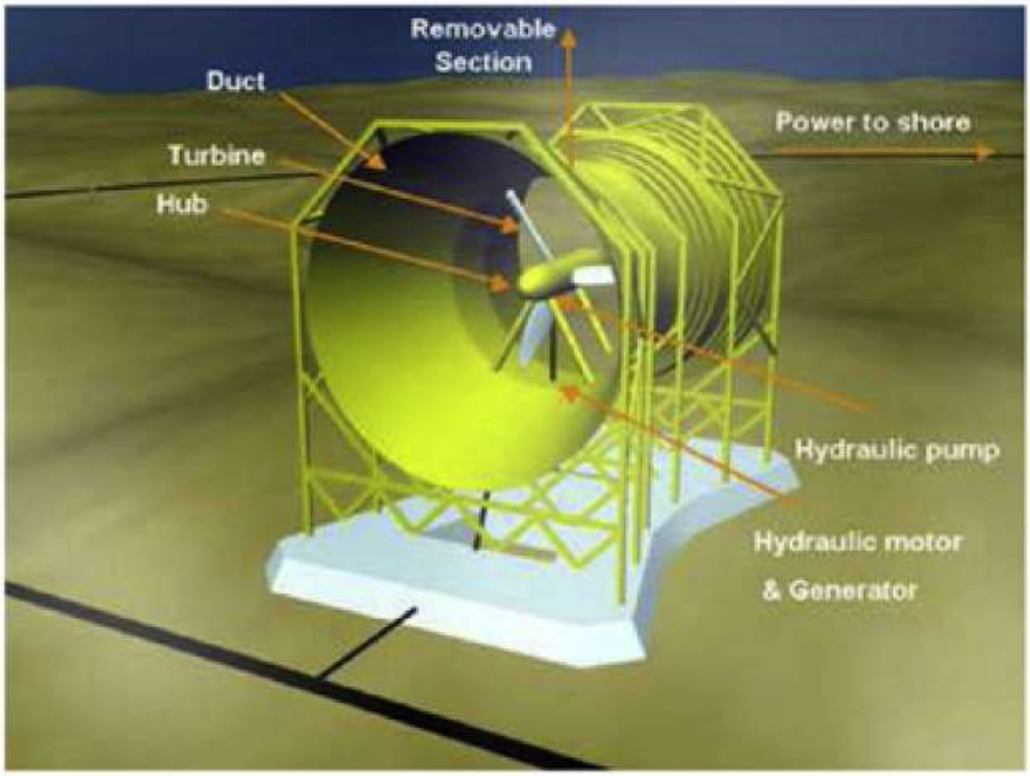

Figure 2.1. Lunar energy's rotech tidal turbine (taken from LunarEnergy-URL 2007)

2.2.2. Permanent Magnet Generator and Induction Generator System. While hydrokinetic turbine converts the kinetic energy stored in the water mass into mechanical energy available at the end of turbine shaft, a device is needed to convert this mechanical energy into electrical energy for further use. Generally, two kinds of generators are used in wind and hydrokinetic turbine systems, permanent magnet synchronous generator and induction generators such as doubly-fed induction generators and squirrel cage induction generators [20]. Permanent magnet synchronous generators are usually employed for low power systems while induction machines are usually employed for high power systems.

A doubly-fed induction generator (DFIG) is also able to supply power at constant voltage and constant frequency while the rotor speed varies, which makes it suitable for grid-tie variable-speed turbine systems [21]. In addition, another big advantage of the DFIG-based system is that the power electronic equipment only needs to handle a fraction of the total system power, usually 20-30%, which reduces the power loss and the cost of power electronic devices [22].

River-based hydrokinetic turbine systems are usually KW level systems which are categorized into low power turbine systems. Therefore PMSG is usually adopted for electrical power generation for river-based hydrokinetic turbine systems.

2.2.3. Power Converters and Control for Hydrokinetic Turbine System. Power converters are necessary in a hydrokinetic turbine system to process the electrical power generated by the generator and in the mean time, control the hydrokinetic turbine operations. Depending on the load type of the system, different power converters are needed.

For a grid-tie hydrokinetic turbine system shown in Fig 1.1, an ac/dc rectifier is used to convert the ac power coming out of the generator in to dc power. Then a dc/dc converter is connected after the rectifier. To interface with the grid, a dc/ac inverter is connected in between the dc/dc converter and the grid. There are two control objectives for grid-tie hydrokinetic turbine system. One is to ensure maximum output power capture of the hydrokinetic turbine. The other one is to ensure the power flow injecting into the grid which requires a constant dc bus voltage on the output side of the dc/dc converter and the grid side current to synchronize with the grid voltage. Since there are two power converters in this kind of system configuration, therefore there are two different control strategies. The first control strategy is illustrated in Fig 2.2. The turbine output power tracking is realized by the dc/dc boost converter while the dc bus regulation and grid current synchronization control is realized by the dc/ac inverter. The second control strategy is illustrated in Fig 2.3. In the second control strategy, the boost converter and the dc/ac inverter have shifted functions in comparison with the first control strategy. The boost converter is used to regulate the dc bus voltage and the dc/ac inverter is used to track the turbine output power and synchronize the grid current. These two control strategies for PMSG grid-tie turbine system are elaborated in [2], and the simulation

results show that both control strategies have the same power control capabilities under rapid wind or water speed changes. However, the second control strategy has a better power control capability compared with the first control strategy under grid fault.

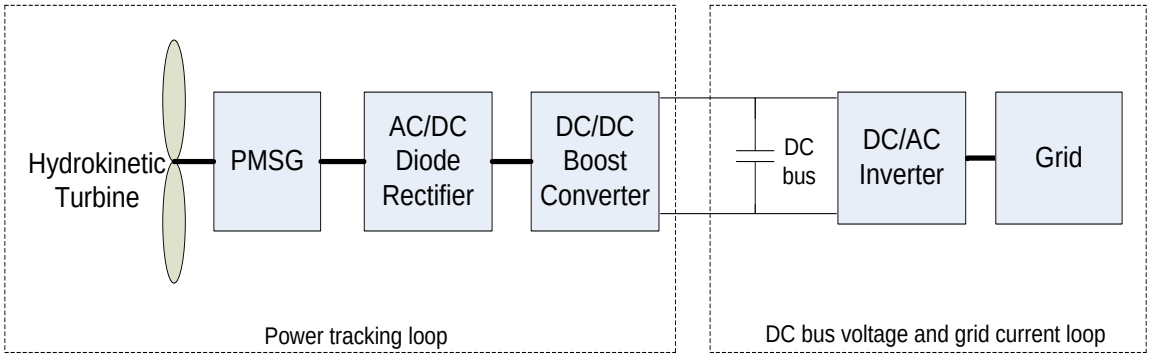

Figure 2.2. Control strategy I of grid-tie hydrokinetic turbine system

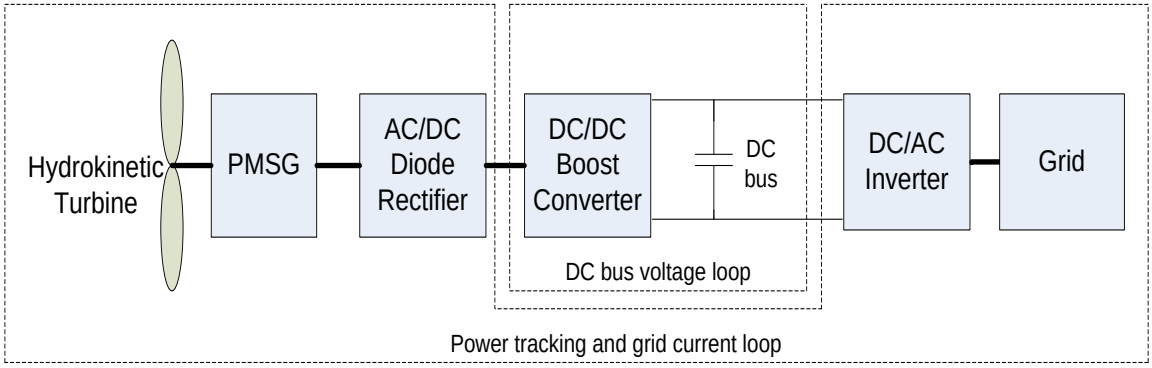

Figure 2.3. Control strategy Π of grid-tie hydrokinetic turbine system

For a stand-alone hydrokinetic turbine system shown in Fig 1.2, an ac/dc rectifier is used to convert the ac power coming out of the generator in to dc power. Then a dc/dc converter is connected in between a battery load and the ac/dc rectifier. This configuration is similar to the grid-tie system except for that a dc/ac inverter is no longer needed and an energy storage device, such as battery is used. Since there is no grid connection, the only control objective for a stand-alone hydrokinetic turbine system is to

ensure the maximum power capture of the hydrokinetic turbine which is shown in Fig 1.3.

2.2.4. System Design for Missouri S&T Hydrokinetic Project. The objective for the Missouri S&T hydrokinetic project is to design a prototype of a river-based hydrokinetic turbine system. The estimated output power of the system is 7.7 w and the system is designed to produce power for individual household without grid interface. The output power is limited by the size of the water tunnel and the hydrokinetic turbine that will be tested in the water tunnel. Based on these preliminary designing objectives, a system level design for this hydrokinetic turbine system is carried out.

First of all, the general turbine type of the system, vertical or horizontal, has to be determined. Even though, vertical turbine system is innovative and allows the generator to be mounted above the water level, the lack of predictability of its performance and the difficulty to integrate water velocity increaser into the system leads to a horizontal axis turbine system. Also, because of the difficulty to connect the generator to the turbine in the water, the generator is mounted on top of a platform that is placed above the water level. This requires a beveling gear to convert the horizontal rotational movement into vertical rotational movement.

Once the turbine type is determined, a generator needs to be selected to convert the mechanical energy into electrical energy. As discussed in section 2.2.2, permanent magnet synchronous generators are usually employed for low power systems, because of its high reliability, simple structure, low noise and high power density. In addition, for PMSG to operate there is no need to add extra field excitation winding like induction generators. Therefore PMSG is used for this system. The selected PMSG needs to coordinate well with the hydrokinetic turbine to achieve good performance of the overall system. Generally speaking, there are two important parameters of the turbine and the generator that needs to be properly coordinated. One parameter is the turbine rotational speed and the generator rotational speed. If a gearbox is not used in between the turbine and the generator, the turbine maximum rotational speed should not exceed the generator maximum rotational speed. In addition, the rated generator speed needs to be close to the operating speed range of the turbine. For example, if the turbine operating speed range is 10 times less than the rated speed of the generator, the overall system is highly inefficient

because the operating speed is far less than the rated speed of the generator. One possible solution is to use a gearbox (speed increaser) in between the turbine and the generator, so that the rotational speed for the generator can be increased to its rated operating speed. The other parameter is the maximum torque of the turbine and the starting torque of the generator. The maximum torque of the turbine has to be greater than the starting torque of the generator otherwise the turbine is not able to drive the generator. A SHINANO KENSHI PMSG which is rated at 80 W and 3000 rpm is selected for this system. Since the rated speed of the selected PMSG far exceeds the operating speed range of the hydrokinetic turbine, a 1:10 ratio speed increaser is built for the system.

After the generator is selected, the next step is to design the power converters for the system. As shown in Fig. 1.2, for stand-alone hydrokinetic turbine systems, a diode rectifier and a boost converter is usually used to process the electrical power flow and a battery is needed to store the generated electrical energy.

In terms of control for the stand-alone prototype hydrokinetic turbine system, maximum power point tracking control is adopted to ensure the maximum capture of the potential hydrokinetic energy which makes the system more cost-effective. The developed MPPT control strategy for the hydrokinetic turbine system is elaborated in section 3.

3. MPPT CONTROL OF STAND-ALONE HYDROKINETIC TURBINE

3.1. INTRODUCTION

A hydrokinetic turbine, like a wind turbine, has the variable speed capability for optimal energy extraction. For different water velocity, the maximum power point for the hydrokinetic turbine occurs at different turbine rotor speed [16]. Therefore, in order to capture the maximum amount of potential energy from the hydrokinetic turbine, the turbine rotational speed has to be optimized.

In medium and large turbine systems, pitch angle control is usually adopted to optimize output power as well as to reduce torque and output power variations for high water speed [17]. However, for small size turbine systems, the mechanical structure limits make pitch angle control unrealistic [13]. Therefore, a power converter is usually adopted to implement the MPPT control in small-scale turbine systems, such as boost converter.

In order to analyze the mechanical and electrical interaction of the hydrokinetic turbine system, detailed mathematical model of each component of the system is studied, based on which an MPPT control method is developed in this section.

3.2. HYDROKINETIC TURBINE MODEL

The developed model is based on the steady-state power characteristics of the hydrokinetic turbine. The output power of a hydrokinetic turbine is given by

$$P_m = 0.5\rho\pi r^2 v^3 C_p(\lambda, \beta) \tag{1}$$

where P_m is the turbine output power, ρ is the water density(997 kg/m3 at 25 °C), r is the blade radius(m), v is the water velocity(m/s), C_p is the power coefficient of the hydrokinetic turbine, λ is the tip speed ratio and β is the pitch angle of the turbine.

Therefore, if the water density ρ, blade radius r and water velocity v are constant, the output power P_m is proportional to the power coefficient C_p which is determined by the value of λ and β. However, for a fixed pitch angle hydrokinetic turbine which is the

main interest of discussion in this thesis, the power coefficient is only determined by λ. Therefore, the output power of a hydrokinetic turbine is given by

$$P_m = 0.5\rho\pi r^2 v^3 C_p(\lambda) \tag{2}$$

The tip speed ratio of a hydrokinetic turbine is defined as

$$\lambda = \frac{r\omega_m}{v} \tag{3}$$

where r is the blade radius(m), v is the water velocity(m/s), and ω_m is the rotational speed of the hydrokinetic turbine(rad/s).

Based on the hydrodynamic analysis of the hydrokinetic turbine used in this hydrokinetic project [26], a simplified relationship between C_p and λ when the pitch angle is 12° is given by

$$C_p = \frac{16}{27}\lambda\left(\lambda + \left(1.32 + \frac{\left(\frac{\lambda-8}{20}\right)^2}{\mathrm{B}^{0.667}}\right)\right)^{-1} - \frac{0.57\lambda^2}{C(\lambda + 0.5\mathrm{B})} \tag{4}$$

where B is the number of blades of the hydrokinetic turbine, which is 3, and C is the ratio of lift coefficient, C_l, to drag coefficient, C_d, which is 30. All of the turbine parameters are based on the hydrodynamic analysis of the hydrokinetic turbine that will be used in this project.

Based on Eqn. (4), the C_p-λ characteristic of the hydrokinetic turbine is shown in Fig. 3.1. The maximum value of C_p is 0.395 which is achieved at λ=5.2.

Figure 3.2 gives the characteristics of the hydrokinetic turbine power coefficient C_p for different values of water speed where V1=1 m/s, V2=0.9 m/s, V3=0.8 m/s, and V4=0.7 m/s. The maximum turbine output power $P_{m\_maximum}$ under different water velocities is achieved at different rotational speed as shown in Fig 3.3.

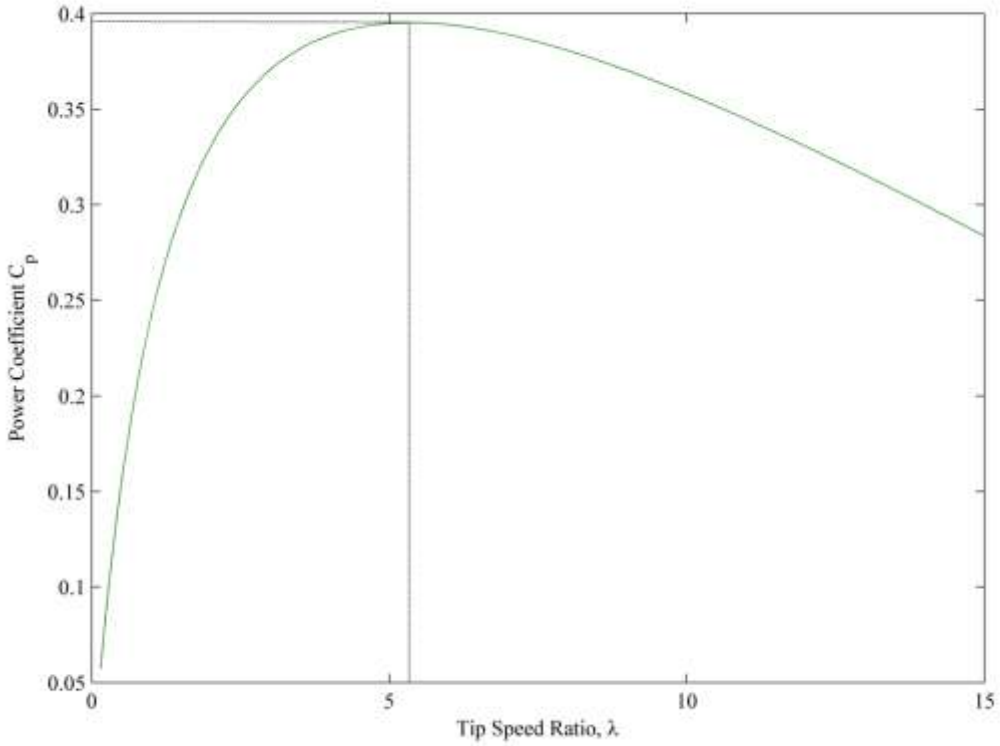

Figure 3.1. C_p-λ characteristic of the hydrokinetic turbine

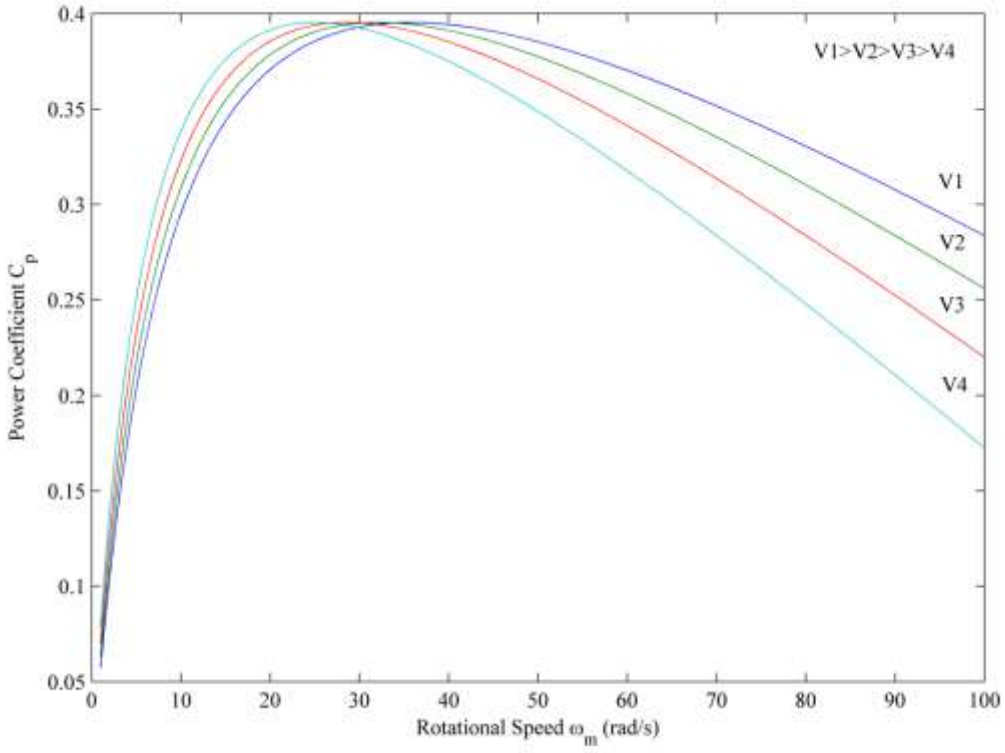

Figure 3.2. C_p-ω_m characteristic of the hydrokinetic turbine at different water speed

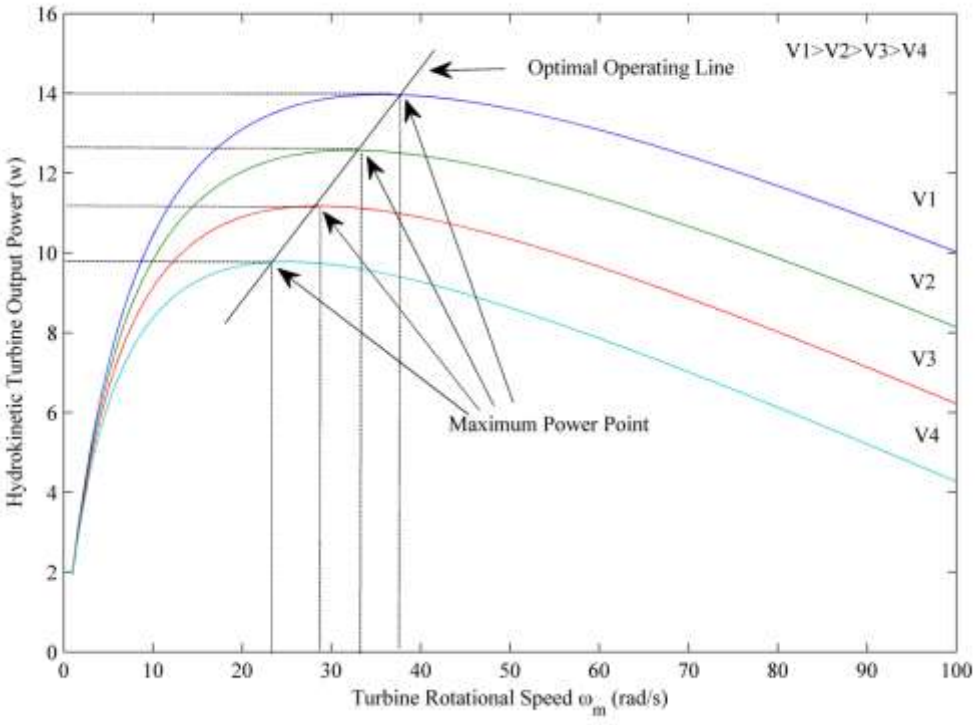

Figure 3.3. P_m-ω_m characteristic of the hydrokinetic turbine at different water speed

3.3. PMSG AND POWER CONVERTER CIRCUIT MODEL

As shown in Fig. 1.2, a typical stand-alone hydrokinetic turbine system consists of a permanent magnet synchronous generator which converts the mechanical power into electrical power, a diode rectifier which converts the ac power into dc power, a dc-dc boost converter which implements the control and battery banks which store the energy generated. In order to analyze the interaction between the mechanical hydrokinetic turbine and the electrical part of the system, a modeling of the PMSG, diode rectifier and the boost converter is necessary. The connection schematic of the PMSG, diode rectifier, boost converter and the battery load is shown in Fig. 3.4. Each phase of the PMSG is modeled as back electromotive force (EMF) *E*, stator resistance *R* and stator inductance *L*. Since the stator resistance *R* is usually small, it is neglected for the analysis in this thesis.

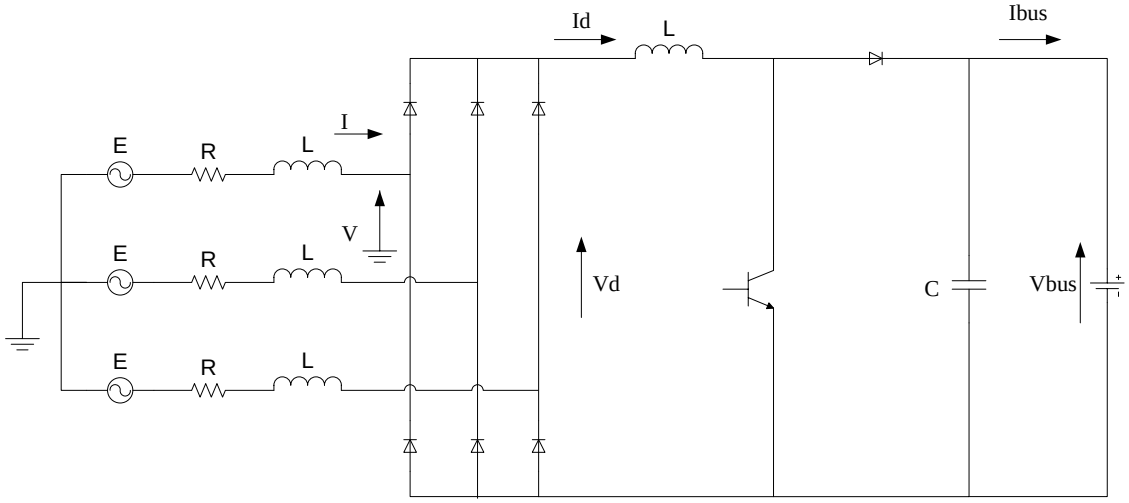

Figure 3.4. Connection circuit of PMSG, diode rectifier, boost converter and battery load

The generated back electromotive force E of PMSG is expressed as

$$E = K\omega_m \tag{5}$$

where K is the back EMF constant of the PMSG, ω_m is the rotational speed of the PMSG.

For each phase of the PMSG, the phase voltage can be written as

$$\hat{\mathrm{E}} = j\omega_e L\hat{\mathrm{I}} + \hat{\mathrm{V}} \tag{6}$$

In terms of magnitude, Eqn. (6) becomes

$$E^2 = (\omega_e LI)^2 + V^2 \tag{7}$$

The relationship between the mechanical frequency ω_m and the electrical frequency ω_e is given by

$$\omega_e = n_p\omega_m \tag{8}$$

where n_p is the number of pairs of poles of the PMSG.

Substituting (5) and (8) into (7), I can be expressed as

$$I = \frac{\sqrt{(K\omega_m)^2 - V^2}}{Ln_p\omega_m} \tag{9}$$

Assuming the power from the generator is converted into dc power through diode rectifier with a unity power factor and that the load current is continuous with no power losses, this yield

$$P_g = 3VI = V_d I_d \tag{10}$$

The mean value of V_d with respect to V_{LL_peak} is given by

$$V_d = \frac{3}{\pi}\int_{-\frac{\pi}{6}}^{\frac{\pi}{6}} V_{LL\_peak}\cos\theta d\theta \tag{11}$$

$$V_d = \frac{3}{\pi}V_{LL\_peak} \tag{12}$$

where V_{LL_peak} is the line to line peak voltage of the PMSG.

Therefore the relationship between V_d and V_{LL} and V can be expressed as

$$V_d = \frac{3}{\pi}\sqrt{2}V_{LL} \tag{13}$$

$$V_d = \frac{3}{\pi}\sqrt{6}V \tag{14}$$

where V_{LL} is the rms value of the line to line voltage of the PMSG and V is the line to neutral voltage of the PMSG.

Substituting (14) into (10), the relationship between I_d and I can be expressed as

$$I_d = \frac{\pi}{\sqrt{6}} I \tag{15}$$

From (9), (10), (14) and (15), P_g can be expressed as

$$P_g = \frac{\pi V_d}{\sqrt{6} L n_p \omega_m} \sqrt{\left(K\omega_m\right)^2 - \left(\frac{\pi V_d}{3\sqrt{6}}\right)^2} \tag{16}$$

From (16), the condition for which the PMSG generates power is obtained

$$\left(K\omega_m\right)^2 - \left(\frac{\pi V_d}{3\sqrt{6}}\right)^2 \geq 0 \tag{17}$$

Solving (17), the minimum speed for which the PMSG generates power is

$$\omega_m \geq \frac{\pi V_d}{3\sqrt{6}K} \tag{18}$$

Therefore, the rotational speed of the generator has to be higher than $\frac{\pi V_d}{3\sqrt{6}K}$ for the generator to generate power.

Figure 3.5 shows the PMSG output power with respect to the generator rotational speed at various values of V_d. The minimum generator rotational speed for which the PMSG starts to generate power is determined by the value of V_d. The higher the V_d, the higher the generator speed is before it starts to export energy. Therefore, in order to produce energy at low water speed, it is necessary to impose a lower value of V_d which can be achieved by using a boost converter.

Figure 3.6 shows the PMSG output power with respect to V_d at different generator rotational speed. For each rotational speed, there is only one optimal value of V_d that

generates the maximum power. Therefore, in order to track the maximum power point, optimal V_d has to be found.

Since a boost converter is used in between the diode rectifier and the load side, the following Eqn. can be obtained

$$\frac{V_{bus}}{V_d} = \frac{1}{1-D} \tag{19}$$

where D is the duty ratio of the boost converter.

Substituting **Error! Reference source not found.** into **Error! Reference source not found.**, P_g can be expressed as

$$P_g = \frac{\pi(1-D)V_{bus}}{\sqrt{6}Ln_p\omega_m}\sqrt{(K\omega_m)^2 - \left(\frac{\pi(1-D)V_{bus}}{3\sqrt{6}}\right)^2} \tag{20}$$

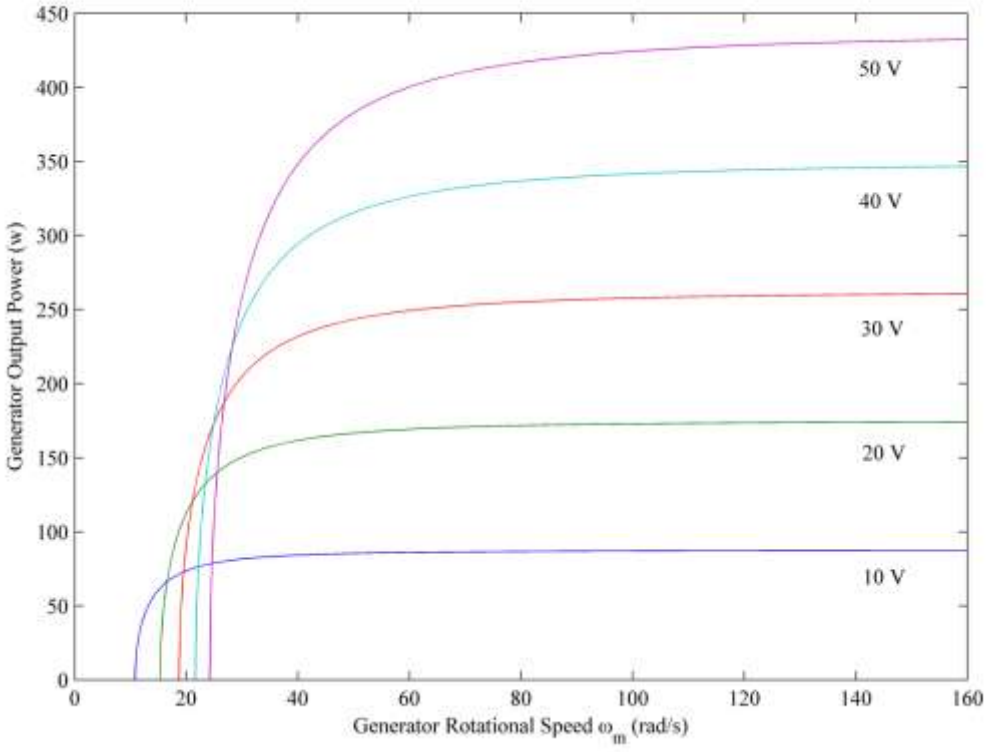

Figure 3.5. P_g-ω_m characteristic at various values of V_d

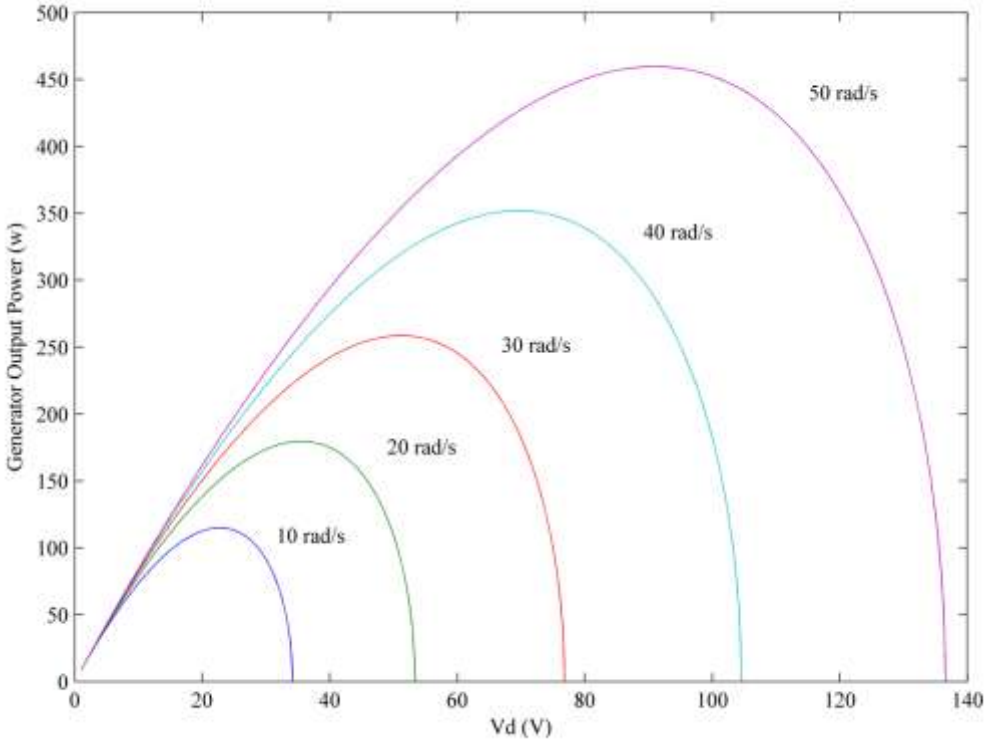

Figure 3.6. P_g-V_d characteristic at different generator rotational speed

Figure 3.7 shows the PMSG output power with respect to duty ratio D at different generator rotational speed when V_{bus}=150 V. For each rotational speed, there is only one duty ratio that would enable the system to generate maximum power. Therefore, the maximum power point tracking is equivalent to tracking the optimal duty ratio. Control of the duty ratio can be achieved by a microcontroller.

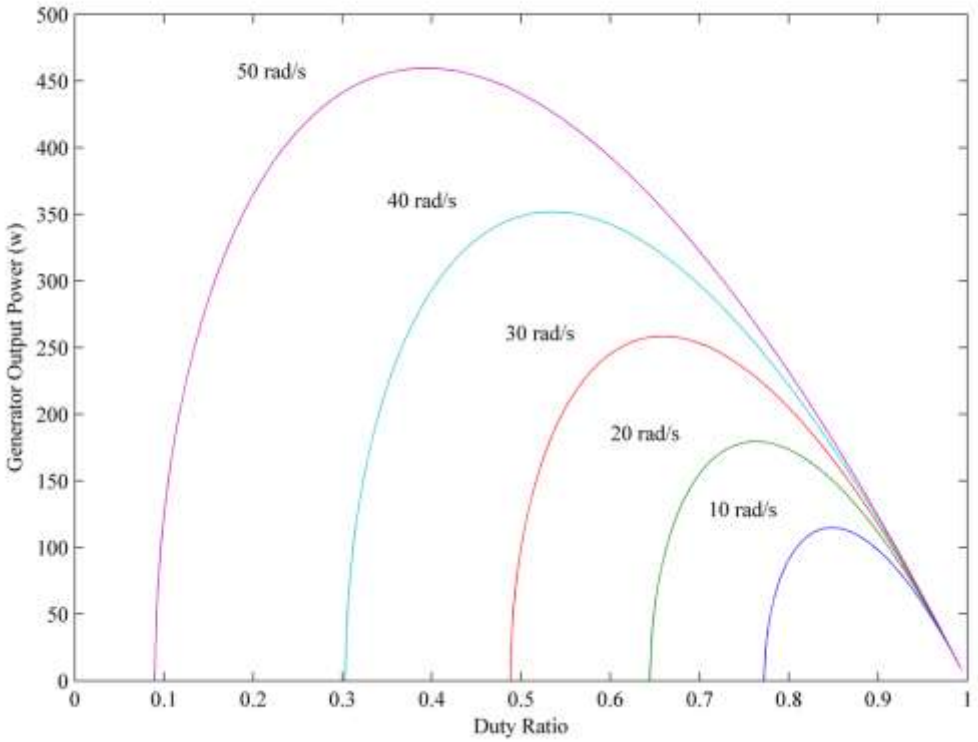

Figure 3.7. P_g-D characteristic at different generator rotational speed

3.4. PROPOSED MPPT CONTROL ALGORITHM

Different hydrokinetic turbines have their own C_p-λ characteristic curve which means for different hydrokinetic turbines, the tip speed ratio for the maximum C_p is different. It is possible to measure the C_p-λ characteristic curve for each turbine. However, this is not a good solution for small-scale hydrokinetic turbines because the cost to measure the C_p-λ characteristic curve for small-scale hydrokinetic turbines is

expensive compared to the system cost itself. Therefore a generic MPPT control algorithm is developed in this thesis which automatically tracks the maximum power point of the turbine without the need to pre-measure the C_p-λ characteristics.

Figure 3.8 shows the flow chart of the proposed MPPT control algorithm. P and D are the measured output power and duty ratio of the boost converter, respectively. K is the step change in duty ratio. Right is a Boolean variable indicating the location of the operating point. When Right is true, the operating speed is higher than the optimal rotor speed. When Right is false, the operating speed is lower than the optimal rotor speed. At the beginning of each interrupt cycle, the current cycle Output Power P[n] is updated. Then based on the state of the Boolean variable Right, duty ratio D is changed differently. When Right is true, if P[n]>P[n-1], where P[n-1] is the output power of the previous cycle, then current cycle duty ratio D[n]=D[n-1]-K where D[n-1] is the duty ratio of the previous cycle, otherwise if P[n]<P[n-1], D[n]=D[n-1]+K and Right needs to be set to false. When Right is false, if P[n]>P[n-1], D[n]=D[n-1]+K, otherwise if P[n]<P[n-1], D[n]=D[n-1]-K and Right needs to be set to true. Since the operating speed range for hydrokinetic turbine is narrower than the operating speed range for wind turbine [16], the hydrokinetic turbine speed change cannot be too big to cause a dramatic output power change which means the duty ratio step change, K, cannot be too big. However, K needs to be big enough to cause a detectable output power change for the proposed MPPT algorithm to work. Therefore, the step change, K, needs to be properly tuned to each hydrokinetic system for the MPPT control to achieve its best performance. For this project, K is 0.025 in simulation and 0.0133 in experimental test. In addition, since the mechanical inertia is much higher than the electrical inertia of the system, the frequency for which P[n] is updated cannot be too high. This is because P[n] is directly determined by the steady state value of ω_m and the mechanical speed ω_m needs time to reach its steady-state value because of the high mechanical inertia. Therefore, the frequency for which P[n] is updated needs to be properly adjusted as well to each hydrokinetic system for the MPPT control to achieve its best performance. For this project, this frequency is 10 Hz simulation and experimental test. This MPPT control method is similar to hill-climbing used as MPPT control in photovoltaic systems [23].

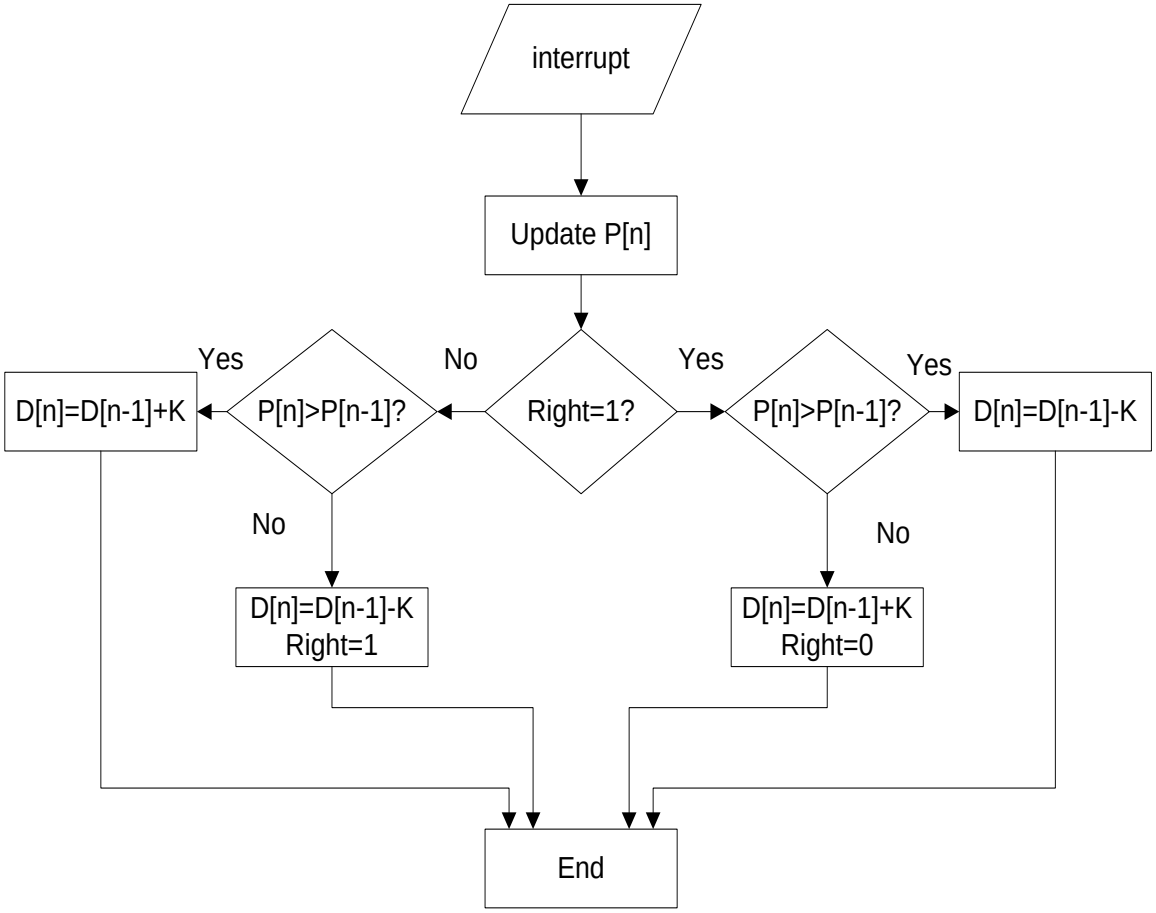

Figure 3.8. Flow chart of the proposed MPPT control algorithm

3.5. SIMULATION RESULTS

The proposed MPPT control is validated by simulation results done in Matlab/Simulink R2010a and PLECS. Figure 3.9 shows the block diagram of the hydrokinetic system built in Matlab/Simulink which consists of the mechanical part (hydrokinetic turbine), the electrical part (generator, diode rectifier, boost converter and battery) and the control part (MPPT).

Figure 3.10 shows the hydrokinetic turbine model built in Matlab/Simulink. Figure 3.11 shows the generator, diode rectifier, boost converter and battery model built in PLECS. The battery bank on the load side is simulated by a constant dc voltage source.

Figure 3.12 shows the block diagram of the MPPT control algorithm built in Matlab/Simulink.

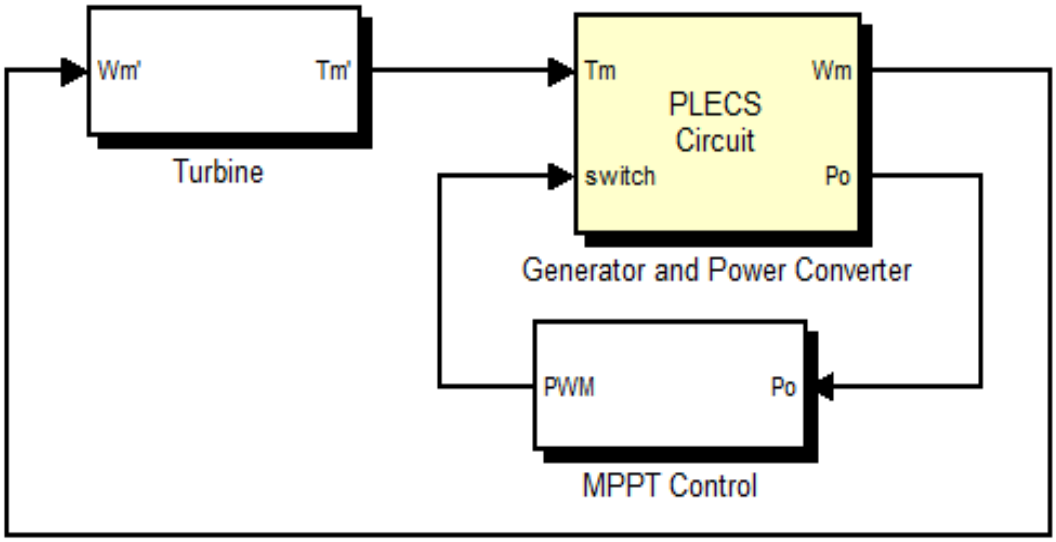

Figure 3.9. Block diagram of the hydrokinetic system built in Matlab/Simulink

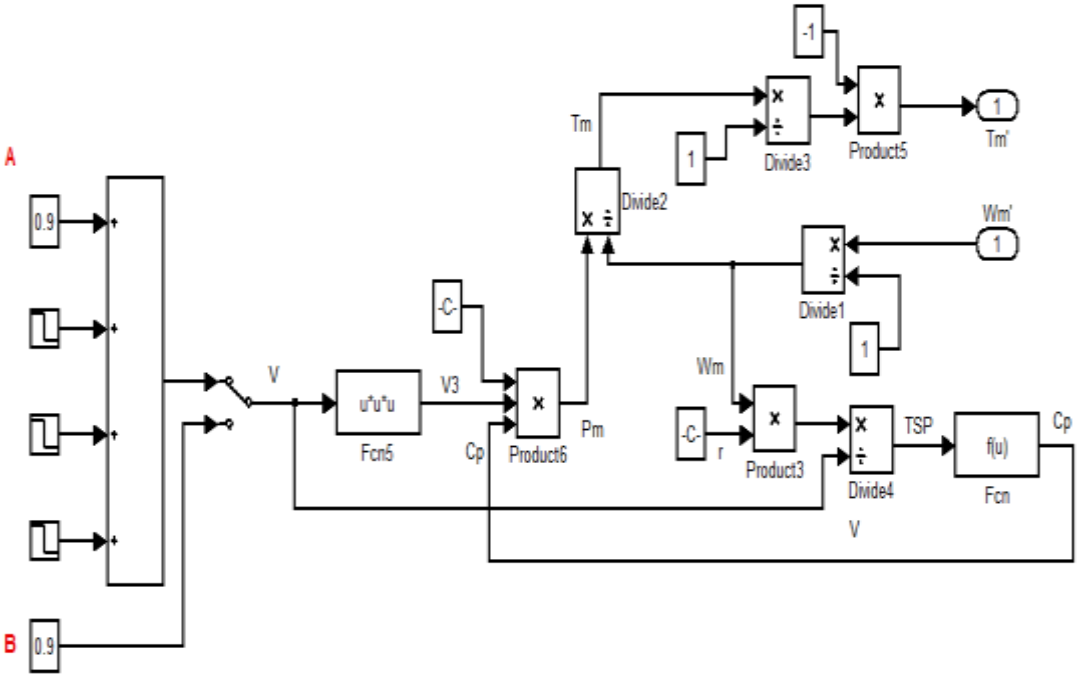

Figure 3.10. Block diagram of the hydrokinetic turbine model built in Matlab/Simulink

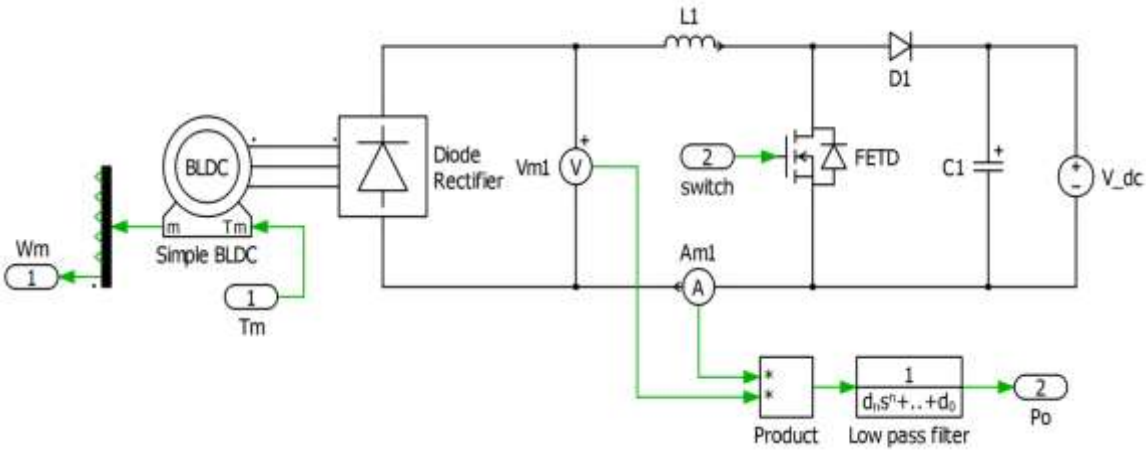

Figure 3.11. Schematic of the generator and power converters built in PLECS

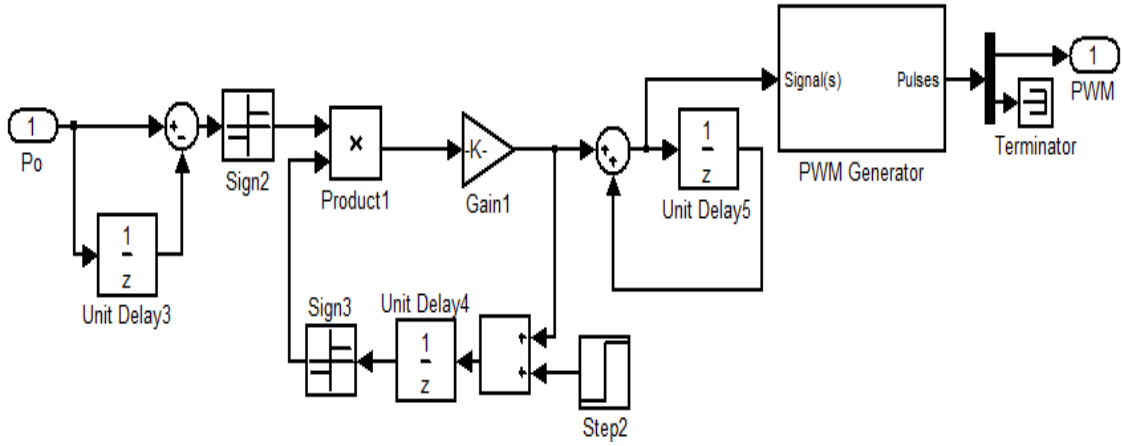

Figure 3.12. Block diagram of the MPPT control built in Matlab/Simulink

The following four different scenarios are simulated:

Case 1 – Hydrokinetic system with fixed duty ratio and fixed water speed

Case 2 – Hydrokinetic system with MPPT control and fixed water speed

Case3 – Hydrokinetic system with fixed duty ratio and water speed variations

Case 4 – Hydrokinetic system with MPPT control and water speed variations

3.5.1. CASE 1: Fixed Water Speed and Duty Ratio. The simplest scenario to operate the hydrokinetic turbine system is when there is no input variations. Therefore the water speed as well as the duty ratio for the boost converter is kept constant. This

operation mode does not take advantage of the variable speed capability for maximum power extraction of the hydrokinetic turbine. Figure 3.13 shows the simulation results of water speed, turbine rotational speed, Cp, torque, duty ratio and the output power. Table 3.1 shows the steady state values of all the parameters in Fig. 3.13.

3.5.2. CASE 2: Fixed Water Speed and MPPT Control. The proposed MPPT control is tested when there is no water speed variations. This scenario is common since water speed tends to be constant. In this case, the proposed MPPT algorithm automatically tracks the optimal duty ratio to change the turbine rotational speed to its optimal value where the maximum C_p occurs. Figure 3.14 shows the simulation results of water speed, turbine rotational speed, C_p, torque, duty ratio and the output power under this scenario. Table 3.2 shows the optimal values of all the parameters in Fig. 3.14. From the steady-state values in table 3.1 and the optimal values from table 3.2, it is proven that at fixed water speed, hydrokinetic turbine system can harvest more potential energy with the proposed MPPT control.

3.5.3. CASE 3: Varied Water Speed and Fixed Duty Ratio. The third operation scenario for the hydrokinetic system is to run it in a varied water speed environment with fixed duty ratio. The rotational speed of the turbine will change because of the water speed change. However, this is not due to the control on the electrical side of the system. The water speed starts at 0.9 m/s. Then it is decreased by 0.1 m/s every second. Figure 3.15 shows the simulation results of water speed, turbine rotational speed, C_p, torque, duty ratio and the output power. Table 3.3 shows the steady state values of all the parameters in Fig. 3.15.

3.5.4. CASE 4: Varied Water Speed and MPPT Control. The most complicated operating mode for the hydrokinetic turbine system is to run it in a varied water speed environment and in the mean time, track the maximum power point of the hydrokinetic turbine under different water speed. Figure 3.16 shows the simulation results of water speed, turbine rotational speed, C_p, torque, duty ratio and the output power under this scenario. Table 3.2 shows the optimal values of all the parameters in Fig. 3.16. The water speed starts at 0.9 m/s and the MPPT control changes the duty ratio to its optimal value to achieve the maximum C_p. However, once the water speed decreased to 0.8 m/s, the previous optimal duty ratio is no longer optimal in this

condition. The proposed MPPT control algorithm can automatically adjust itself to the change of water speed and change the value of D until it is optimal again. From the steady-state values in table 3.3 and the optimal values from table 3.4, one conclusion can be drawn that even with water speed variations hydrokinetic turbine system can harvest more potential energy with the proposed MPPT control.

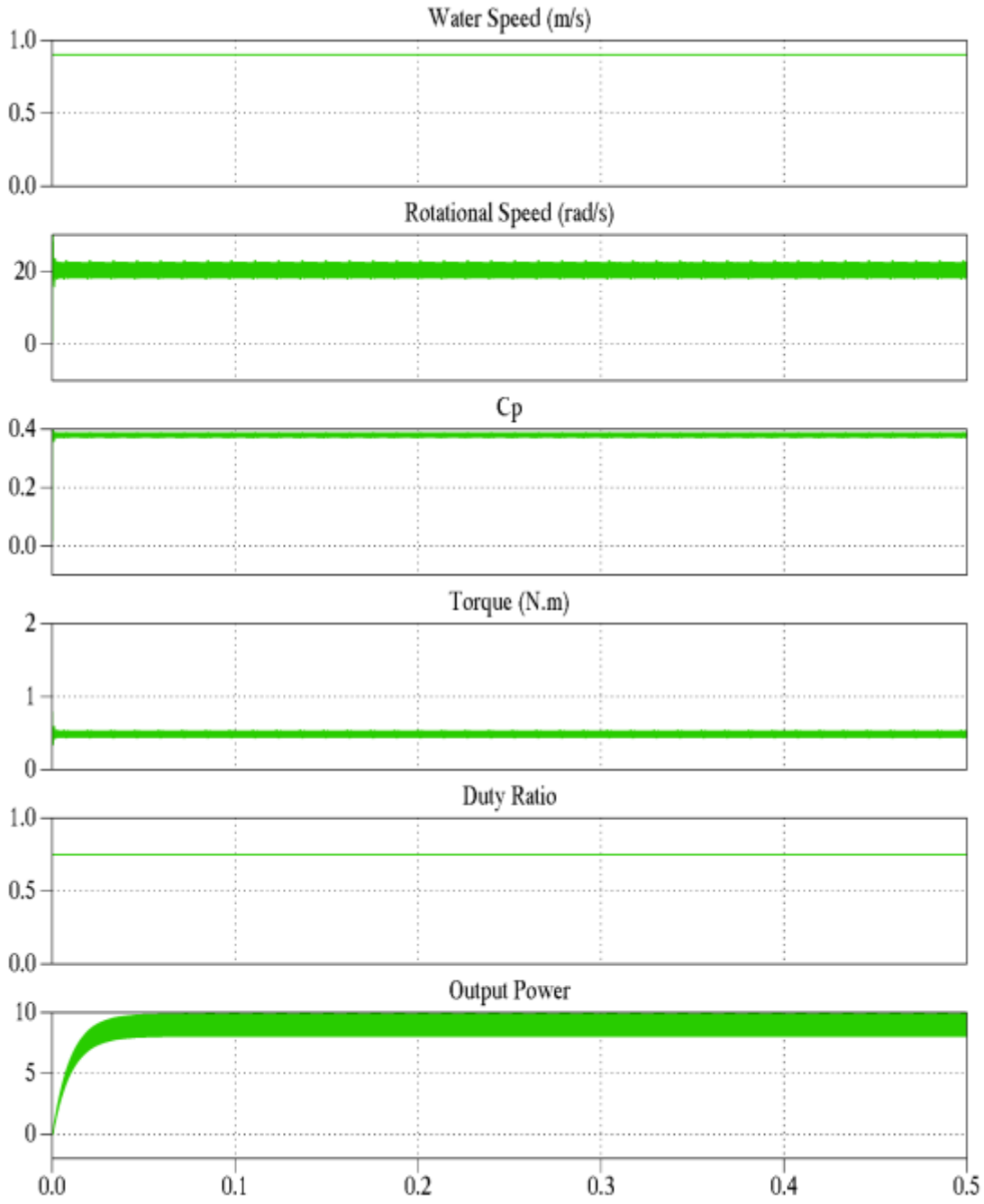

Figure 3.13. Simulation results with fixed water speed and duty ratio

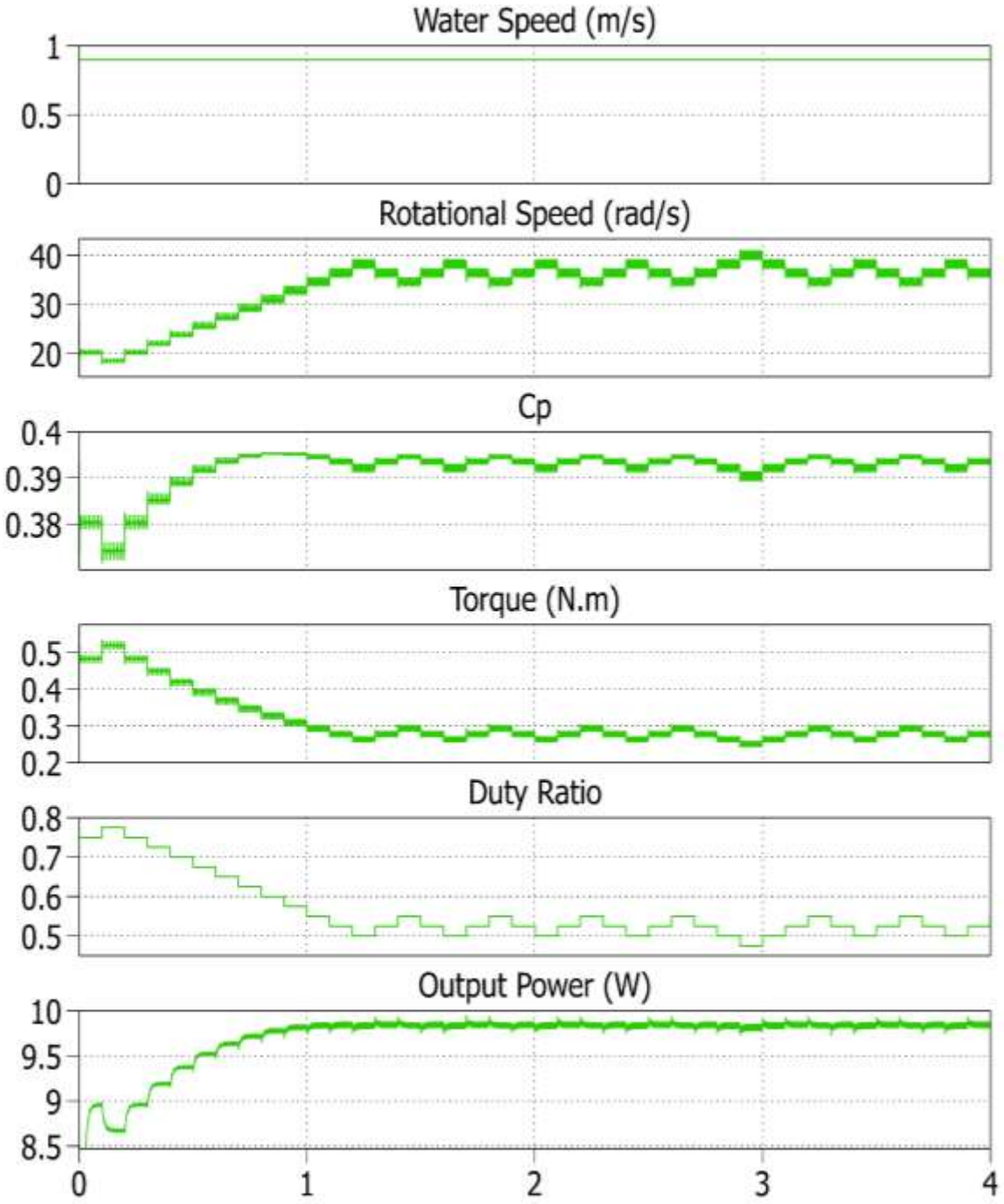

Figure 3.14. Simulation results with fixed water speed and MPPT control

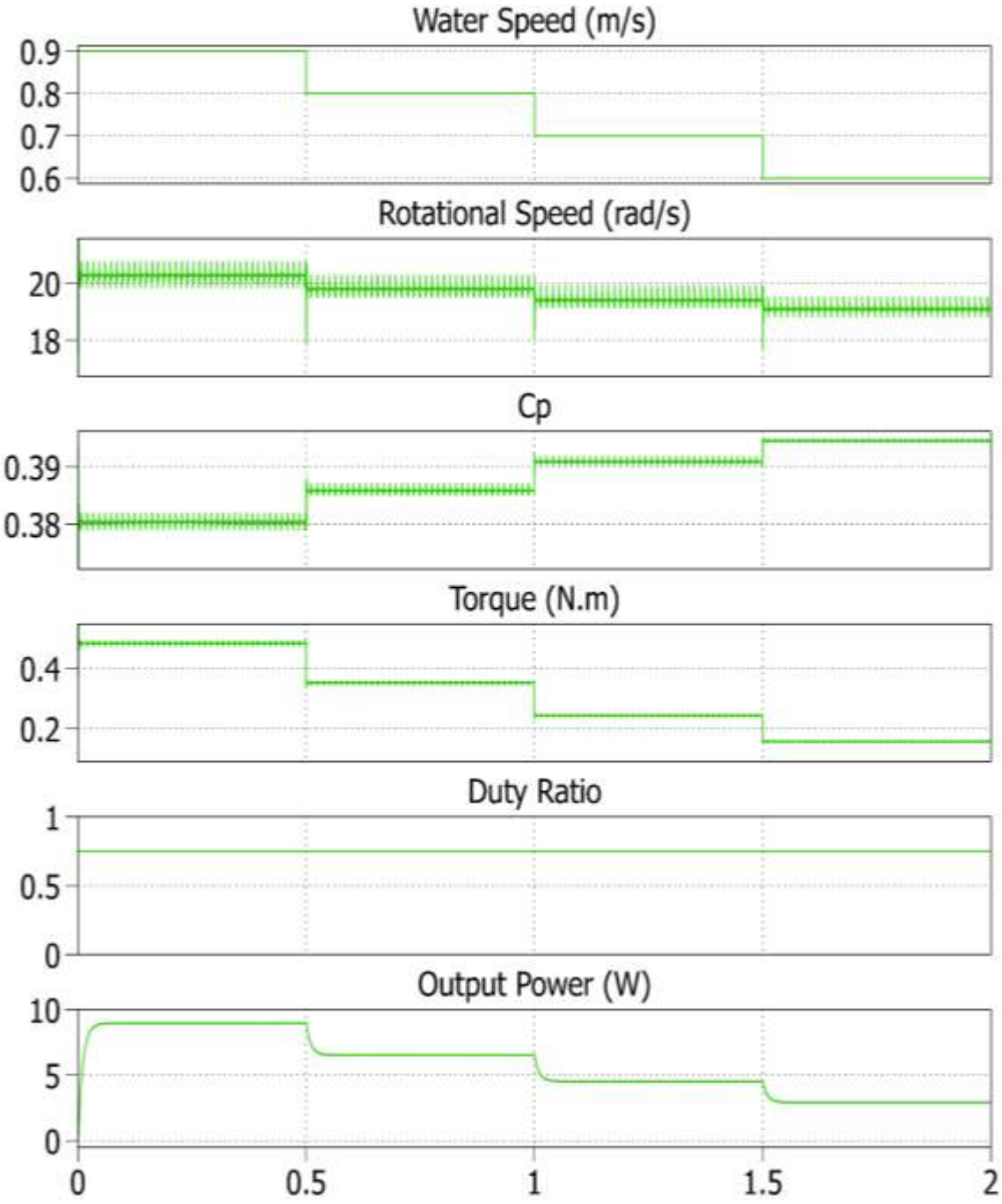

Figure 3.15. Simulation results with varied water speed and fixed duty ratio

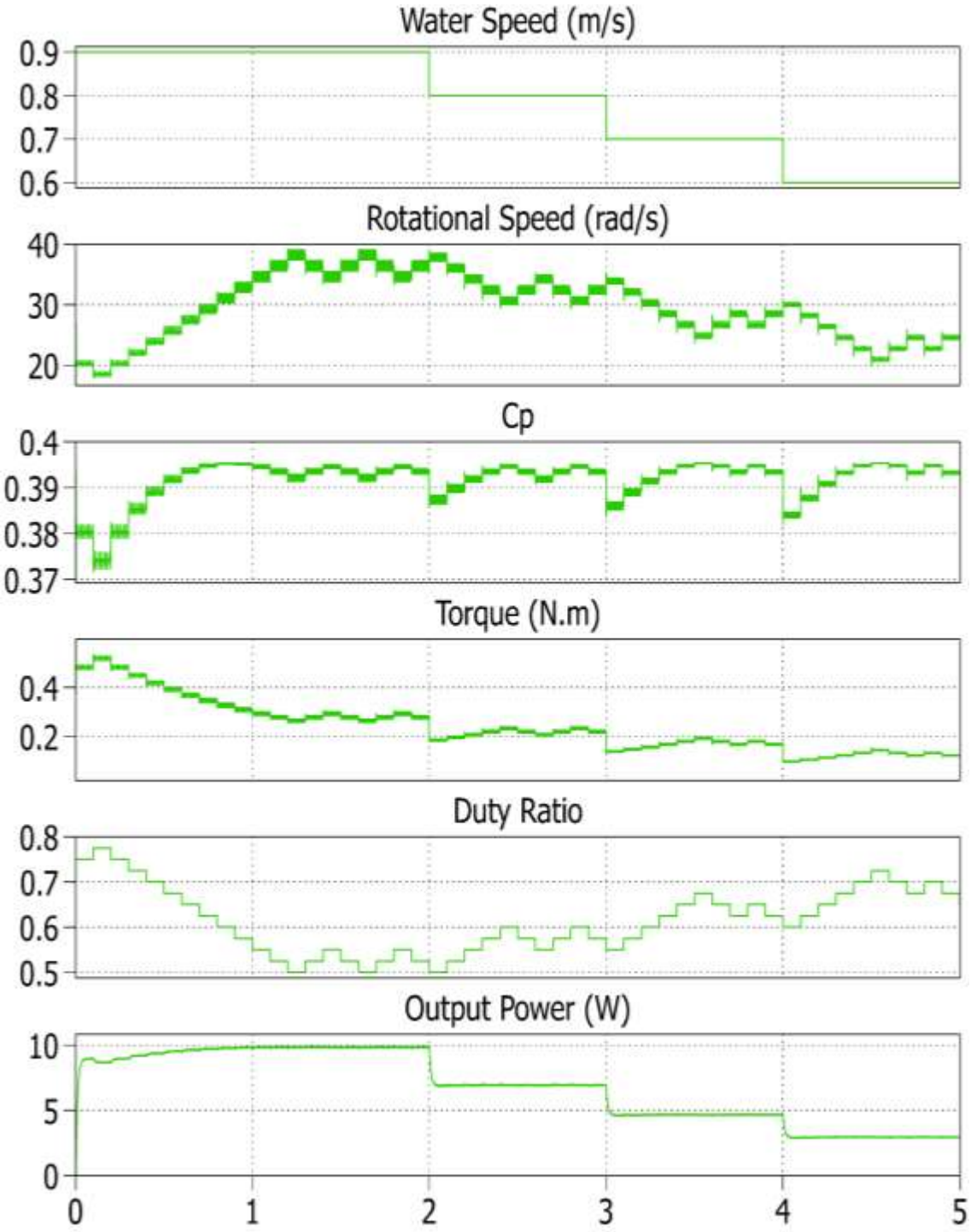

Figure 3.16. Simulation results with varied water speed and MPPT control

Table 3.1. Steady-state value of the parameters of the hydrokinetic system in case 1

Water speed	0.9 m/s
Turbine rotational speed	20.3 rad/s
Power coefficient C_p	0.38
Torque	0.716 N.m
Duty ratio	0.75
Output power	8.96 W

Table 3.2. Optimal value of the parameters of the hydrokinetic system in case 2

Water speed	0.9 m/s
Optimal turbine rotational speed	34.45 rad/s
Maximum power coefficient C_p	0.395
Optimal torque	0.295 N.m
Optimal duty ratio	0.55
Maximum output power	9.84 W

Table 3.3. Steady-state value of the parameters of the hydrokinetic system in case 3

Water speed	0.9 m/s	0.8 m/s	0.7 m/s	0.6 m/s
Turbine rotational speed	20.3 rad/s	19.8 rad/s	19.4 rad/s	19.1 rad/s
Power coefficient C_p	0.38	0.386	0.391	0.394
Torque	0.716 N.m	0.352 N.m	0.243 N.m	0.157 N.m
Duty ratio	0.75	0.75	0.75	0.75
Output power	8.96 W	6.53 W	4.52 W	2.92 W

Table 3.4. Optimal value of the parameters of the hydrokinetic system in case 4

Water speed	0.9 m/s	0.8 m/s	0.7 m/s	0.6 m/s
Optimal turbine rotational speed	34.45 rad/s	30.51 rad/s	24.79 rad/s	20.9 rad/s
Maximum power coefficient C_p	0.395	0.395	0.395	0.395
Optimal torque	0.295 N.m	0.234 N.m	0.193 N.m	0.144 N.m
Optimal duty ratio	0.55	0.6	0.675	0.725
Maximum output power	9.84 W	6.93 W	4.65 W	2.94 W

3.6. EXPERIMENTAL RESULTS

Experimental data are obtained through lab testing of a hydrokinetic turbine system shown in Fig. 1.3. The experimental setup is shown in Fig. 3.17. Experiments are conducted in a controlled environment where the water speed can be controlled and measured. The maximum water speed for the water tunnel used in this experimentation is 0.9 m/s. The constructed PCB board of the diode rectifier and the boost converter is shown in Fig. 3.18. The hydrokinetic turbine is used to drive the PMSG to generate electrical power. However, the turbine rotational speed is too slow to drive the PMSG used for the experimentation. Therefore, a 1:10 speed increaser is used in between the hydrokinetic turbine and the PMSG. The output of the PMSG is connected to the input of the diode rectifier and the output of the boost converter is connected to a constant voltage electronic load which is used to simulate a battery load. In order to measure the input voltage and current of the boost converter, a Texas Instruments TMS320F28335 microcontroller is used. However, the input range of voltage signals for the ADC converter of DSP 28335 is 0-3 V. Therefore a circuit that changes the voltage and current signal into the allowable 0-3 V is required. This circuit is also constructed on the PCB board shown in Fig. 3.18. In addition, the rotational speed is measured by a 400 ppr encoder that is attached to the end of the generator.

In order to validate the proposed MPPT control for the hydrokinetic turbine system, the following experiment procedures are adopted. First the P-ω_m characteristic of the hydrokinetic turbine for different water speed is measured by manually varying the duty ratio from 0 to 1. Then the MPPT control algorithm is implemented in the DSP 28335 microcontroller to automatically track the maximum power points. The maximum power obtained by manually changing the duty ratio is then compared with the maximum power obtained by implementing the MPPT control.

First the turbine power characteristic is tested when the water speed is 22 inches/s with the output voltage regulated at 9.97 V. The test results are shown in Table 3.5. Then the turbine power characteristic is tested when the water speed is 26 inches/s with the same output voltage of 9.97 V and the test results are shown in Table 3.6. Based on the test results, the turbine P-ω_m characteristics under these two different water speed are drawn in Fig. 3.19. Also the test results show that when V_{water}=22 inches/s, the maximum

output power is 1.345 W and this happens when the turbine rotational speed is around 45 rpm and the optimal duty ratio is 0.467. When V_{water}=26 inches/s, the maximum output power is 2.765 W and this happens when the turbine rotational speed is around 62 rpm and the optimal duty ratio is 0.507.

Table 3.5. Test results of the hydrokinetic system with V_{water}=22 inches/s, V_{out}=9.97V

Turbine rotation speed (rpm)	Duty ratio	Output Voltage (V)	Output Current (A)	Output Power (W)
59	0	9.97	0.076	0.75772
57	0.06666667	9.97	0.097	0.96709
55	0.13333333	9.97	0.108	1.07676
53	0.2	9.97	0.119	1.18643
51	0.26666667	9.97	0.125	1.24625
49	0.33333333	9.97	0.128	1.27616
47	0.4	9.97	0.133	1.32601
45	0.46666667	9.97	0.135	1.34595
43	0.53333333	9.97	0.127	1.26619
41	0.6	9.97	0.115	1.14655
39	0.66666667	9.97	0.097	0.96709
37	0.73333333	9.97	0.083	0.82751
34	0.8	9.97	0.061	0.60817
32	0.86666667	9.97	0.046	0.45862

Figure 3.17. Lab setup for experimentation

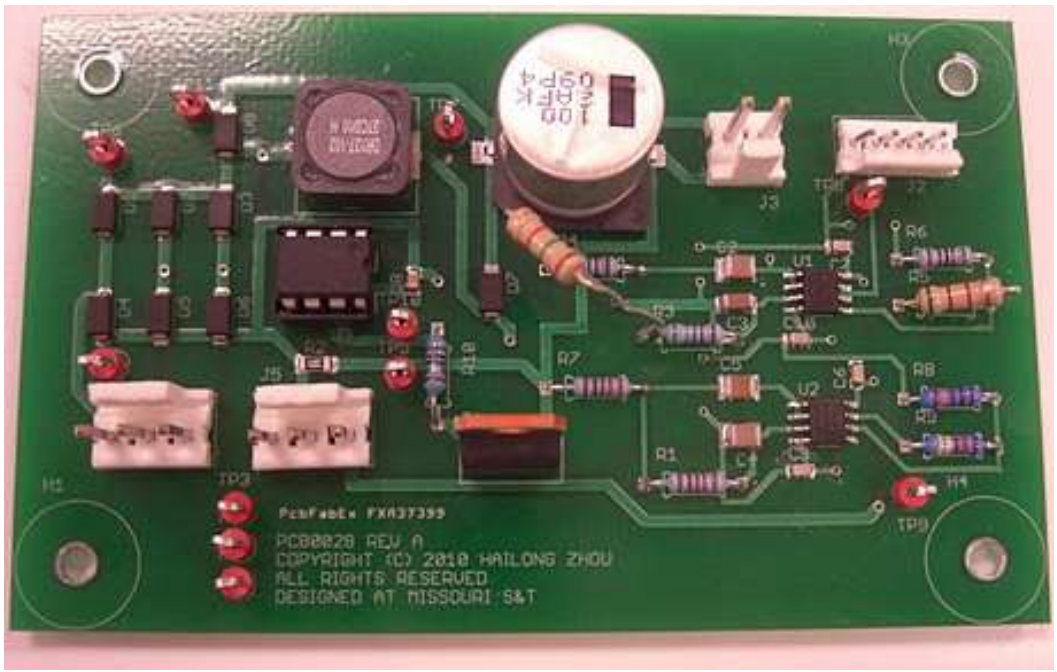

Figure 3.18. PCB board of the diode rectifier and boost converter

Table 3.6. Test results of the hydrokinetic system with V_{water}=26 inches/s, V_{out}=9.97V

Turbine rotation speed (rpm)	Duty ratio	Output Voltage (V)	Output Current (A)	Output Power (W)
81	0	9.97	0.0540903	0.53928
78	0.06666667	9.97	0.106678	1.06358
76	0.13333333	9.97	0.1382307	1.37816
74	0.2	9.97	0.1818034	1.81258
72	0.26666667	9.97	0.2223711	2.21704
69	0.33333333	9.97	0.2464112	2.45672
67	0.4	9.97	0.2614363	2.60652
64	0.46666667	9.97	0.2764614	2.75632
62	0.507	9.97	0.277332	2.765
61	0.53333333	9.97	0.2689488	2.68142
58	0.6	9.97	0.2494102	2.48662
55	0.66666667	9.97	0.2283811	2.27696
52	0.73333333	9.97	0.1908185	1.90246
48	0.8	9.97	0.1472457	1.46804
44	0.86666667	9.97	0.0991655	0.98868

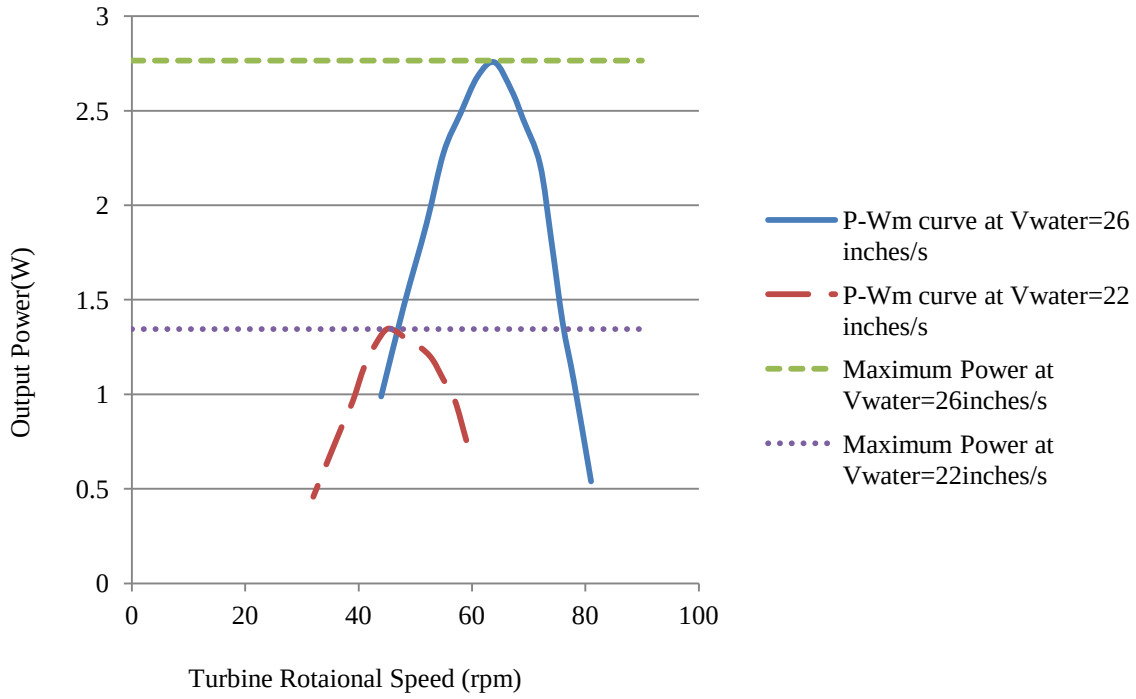

Figure 3.19. Experimental results of P-ω_m characteristics of hydrokinetic turbine under two different water speed

Then the hydrokinetic turbine system is tested with the proposed MPPT control implemented in the boost converter under V_{water}=22 inches/s and V_{water}=26 inches/s with the output voltage regulated at 9.97 V. For each water speed, 10 sample points of the output power are collected. The test results are shown in Table 3.7 and Table 3.8. Figure 3.20 shows the test results of the output power with MPPT control compared with the maximum output power obtained by manually changing the duty ratio from 0 to 1. The experiment results show that under V_{water}=22 inches/s, the output power of the system oscillates around 1.345 W and that under V_{water}=26 inches/s, the output power of the system oscillates around 2.765 W, both of which are the maximum output power under each water velocity. These experimental results validate the performance of the proposed MPPT control for hydrokinetic turbine system and its power control capability.

Table 3.7. Test results of the hydrokinetic system with MPPT when V_{water}=22 inches/s, V_{out}=9.97V

sample	Rotating speed (rad/s)	Output power (W)
1	45.3	1.291
2	45.9	1.345
3	45.5	1.325
4	46.5	1.333
5	46.3	1.339
6	46.8	1.314
7	45.8	1.334
8	45.5	1.311
9	46.1	1.344
10	46.6	1.326

Table 3.8. Test results of the hydrokinetic system with MPPT when V_{water}=26 inches/s, V_{out}=9.97V

sample	Rotating speed (rad/s)	Output power (W)
1	62.5	2.71
2	62.2	2.754
3	62.7	2.701
4	61.9	2.758
5	61.5	2.712
6	61.3	2.698
7	61.8	2.751
8	62	2.762
9	62.4	2.743
10	62.8	2.733

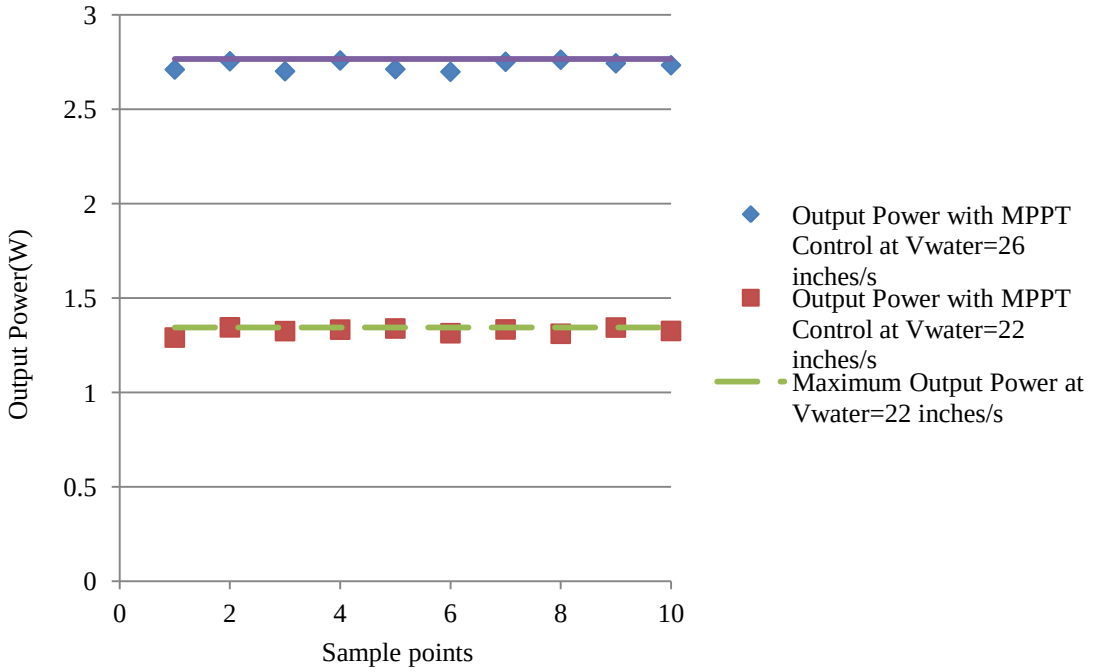

Figure 3.20. Experimental results of output power of hydrokinetic turbine with MPPT control under two different water speed

4. HIGH-THRUST LOW-SPEED PERMANENT MAGNET SYNCHRONOUS GENERATOR DESIGN

4.1. STRUCTURE DESIGN OF PMSG

PMSG has been widely used in small-scale wind and hydrokinetic turbine systems because of its high reliability, simple structure, low noise and high power density. In addition, due to recent developments in permanent magnet materials, especially Nd-Fe-B, high efficiency PMSGs can be manufactured for turbine system applications [24]. Traditionally, the PMSG and the turbine are connected by a gearbox to increase the rotational speed for the PMSG because the rated operating speed of the PMSG is usually much higher than the operating speed of the turbines. However, it is difficult to make the efficiency of speed increaser gearbox very high, which adds additional power transmission losses in the turbine system. Therefore, designing a direct drive PMSG for hydrokinetic system becomes an important issue in hydrokinetic turbine systems [25].

In terms of designing a direct drive PMSG for hydrokinetic turbine system, there are a few objectives and requirements that need to be met. First of all, the PMSG designed has to be capable of producing the rated power for the hydrokinetic turbine at the rated speed of the hydrokinetic turbine, which is usually very low. This requires a high-thrust low-speed PMSG design. Second of all, the efficiency of the designed PMSG has to be high enough so that the direct drive configuration can surpass the gearbox configuration in terms of overall system efficiency.

There are two primary parts for a PMSG, the rotor which is the rotating part, and the stator which is the stationary part. The main component of the stator is the stator winding and the main component of the rotor is the permanent magnet. Depending on the placement of the stator and the rotor, there are two different structure designs for PMSG. Configuration I is the inner rotor and outer stator design as shown in Fig. 4.1 which is a 4-pole 12-slot machine. Configuration II is the outer rotor and inner stator design as shown in Fig. 4.2 which is a 4-pole 24-slot machine.

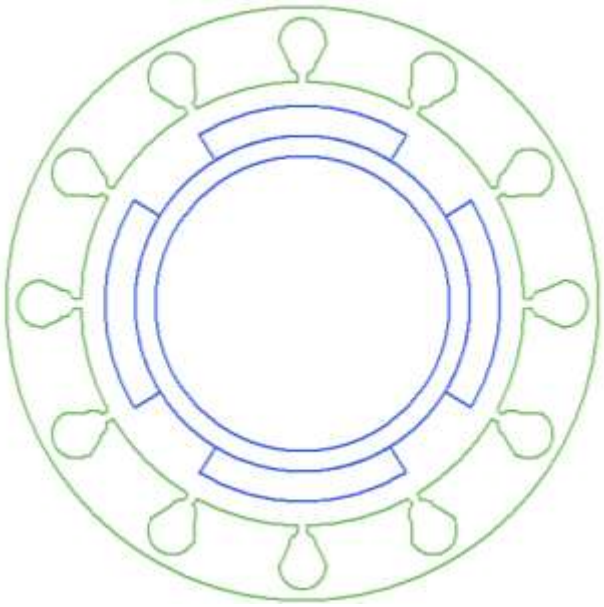

Figure 4.1. Configuration I: Inner rotor and outer stator design

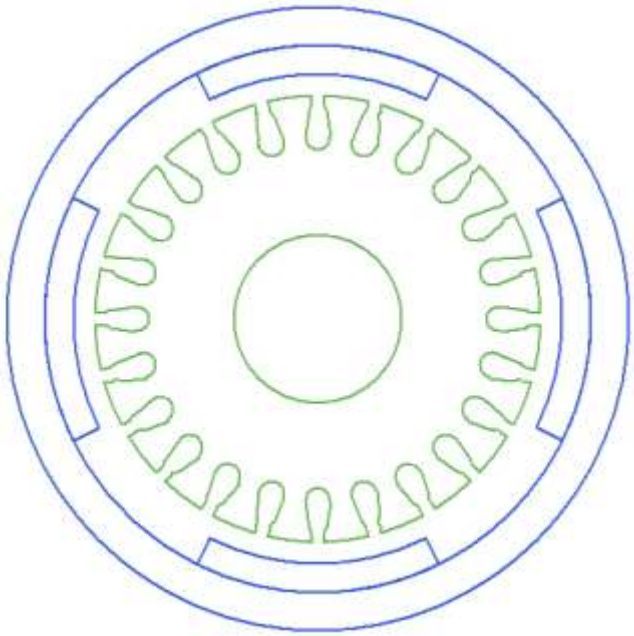

Figure 4.2. Configuration II: Outer rotor and inner stator design

Most of the PMSGs in the market use configuration I, because when the PMSG operates, the stator current going through the stator winding would cause the stator

temperature to go up. Therefore, in order to dissipate all the heat caused by the stator current more effectively, the stator is placed on the outer side because the rotor magnets act as insulators when placed on the outer side. Furthermore, in terms of assembling the generator together and coupling with the turbine shaft, configuration I is simpler than Configuration II.

However, for the hydrokinetic turbine applications, configuration II has several advantages. First of all, the large rotor moment of inertia can ensure smooth operation with small torque variations. In addition, configuration II can minimize the size of stator, reducing the copper needed for stator winding which ultimately reduces the stator resistance and stator inductance, improving the overall efficiency of the PMSG. Therefore, configuration II is adopted for hydrokinetic turbine system applications taking into account of all the advantages it has for this specific application.

4.2. DESIGN PROCEDURE OF PMSG

There are a lot of different parameters that need to be considered in terms of designing a PMSG such as the number of poles, rotor position, stator length and diameters, rotor length and diameters, stator slot type, stacking factor and so on. Rotational Machine Expert (RMxprt) is a template-based electrical machine design tool that provides fast, analytical calculations of machine performance and 2-D and 3-D geometry creation for detailed finite element calculations in ANSYS Maxwell. This software streamlines the design procedure of PMSG, therefore is used to design a PMSG for the hydrokinetic turbine system.

Before designing a PMSG, some turbine information has to be known such as the turbine maximum output power and turbine maximum rotational speed. The design objective of the PMSG is to make sure that the PMSG can generate the maximum output power of the turbine below the maximum rotational speed of the turbine with a high efficiency. Based on the hydrodynamic analysis of the hydrokinetic turbine that will be used in the water tunnel testing, the estimated maximum turbine output power is 7.7 w and the estimated maximum turbine speed is 240 rpm. Therefore, a PMSG that generates 7.7 w of power below 240 rpm needs to be designed which is a high-thrust low-speed machine. Traditionally, a disc type machine (the diameter of the machine is much larger

than the length of the machine) can get better high-thrust low-speed performance. However, for hydrokinetic turbine application, the size of the PMSG is limited by the size of the hydrokinetic turbine. Generally speaking, the diameter of the generator needs to be less than one tenth of the diameter of the hub of the hydrokinetic turbine. Since the diameter of the hydrokinetic turbine that can be tested for the water tunnel cannot exceed 304.8 mm, the maximum diameter for the PMSG is 30.48 mm. However, this diameter limitation poses a big challenge to design a PMSG to generate 7.7 w below 240 rpm. An exception has to be made to increase the diameter of the PMSG which is 70 mm in this case. Figure 4.3 shows the designing template of a PMSG in RMxprt. The property windows are accessed by clicking each of the machine elements, for example, stator, rotor and shaft. All the parameters of the PMSG need to be defined in the property windows, and then the designed machine needs to be simulated in RMxprt. If the simulation results do not meet the designing requirements, then the designer needs to keep changing some of the parameters of the machine and simulating the designed machine until the designing requirements are met.

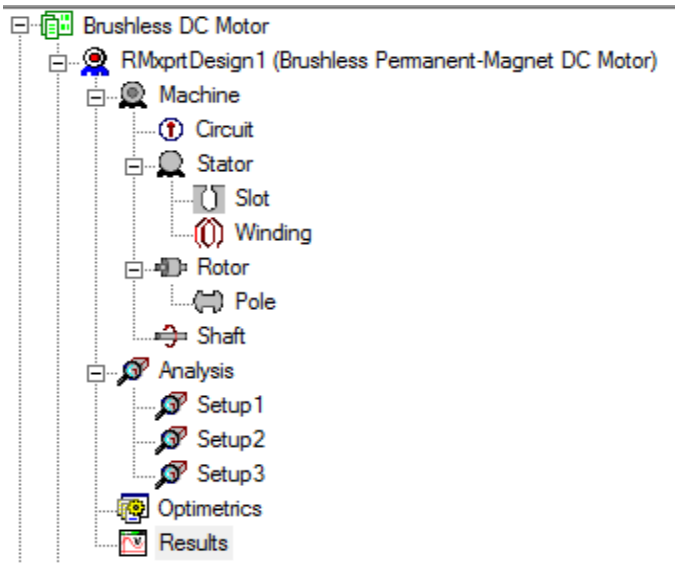

Figure 4.3. PMSG design template in RMxprt

In the Machine properties window, the machine type is defined as Brushless Permanent Magnet DC Motor. The number of poles is defined as 8. Rotor position is chosen to be outer rotor structure, the reason of which is explained in section 4.1. The frictional loss and windage loss is neglected because of their small values and the reference speed is chosen to be the maximum rotational speed of the PMSG which is 240 rpm.

In the rotor properties window, the outer diameter is defined as 70 mm. The inner diameter is defined as 55 mm. The length is defined as 76.2 mm which is close to the diameter of the machine. The stacking factor is estimated to be 0.95 and the pole type is defined as surface mount magnet.

In the pole properties window, the pole embrace is estimated to be 0.56, and the magnet thickness is defined as 3.175 mm. The magnet material is chosen to be Nd-Fe-B.

In the stator properties window, the outer diameter is defined as 50 mm since it has to be smaller than the inner diameter of the rotor and this gives an air gap of 2.5 mm. The inner diameter is defined as 19 mm. The length is defined as 76.2 mm. The stacking factor is again estimated to be 0.95. Total number of slots is chosen to be 24.

In the slot properties window, the exact shape and dimension of the slot can be defined.

In the winding properties window, the winding type is defined as whole-coiled. The number of conductors per slot is chosen to be 35.

Figure 4.4 shows the cross section of the designed PMSG after all the parameters are defined. Figure 4.5 shows the stator winding configurations of the designed PMSG.

4.3. SIMULATION RESULTS

4.3.1. RMxprt Simulation. Once all the parameters of the PMSG are defined a solution setup needs to be added to simulate the designed PMSG. Solution setup is defined in the analysis properties window. The load type is defined as constant speed load. The rated output power and speed is defined as 7.7 W and 240 rpm respectively. The rated DC voltage is 18 Volts. Figure 4.6 shows the simulation results of the output power of the PMSG vs. the rotational speed. The maximum output power is 11.8 W at 145 rpm. There are two different operating points that the generator can output 7.7 W,

230 rpm and 60 rpm. This simulation result meets the requirement of being able to generate 7.7 W below 240 rpm. Figure 4.7 shows the efficiency vs. the rotational speed. At 240 rpm, the generator efficiency is around 80%. Figure 4.8 shows the air gap flux density. The peak value of the air gap flux density is 650 mT. Figure 4.9 shows the induced phase voltage and the induced line voltage of the generator. The peak value of the phase voltage and the line voltage is 9.3 V and 16.1 V respectively. Figure 4.10 shows the cogging torque of the designed PMSG. Table 4.1 shows the simulation results of some of the important parameters of the designed PMSG.

Table 4.1. Parameters of the designed PMSG

Number of poles	8
Armature leakage inductance	2.17 mH
Armature phase resistance	3.32 Ohm
D-axis inductance	3.529 mH
Q-axis inductance	3.529 mH
Maximum speed	300 rpm
Cogging torque	0.0846 N.m

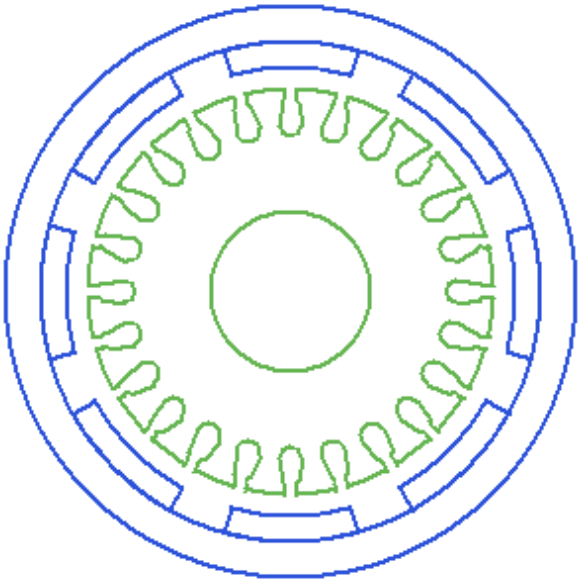

Figure 4.4. Cross section view of the designed PMSG

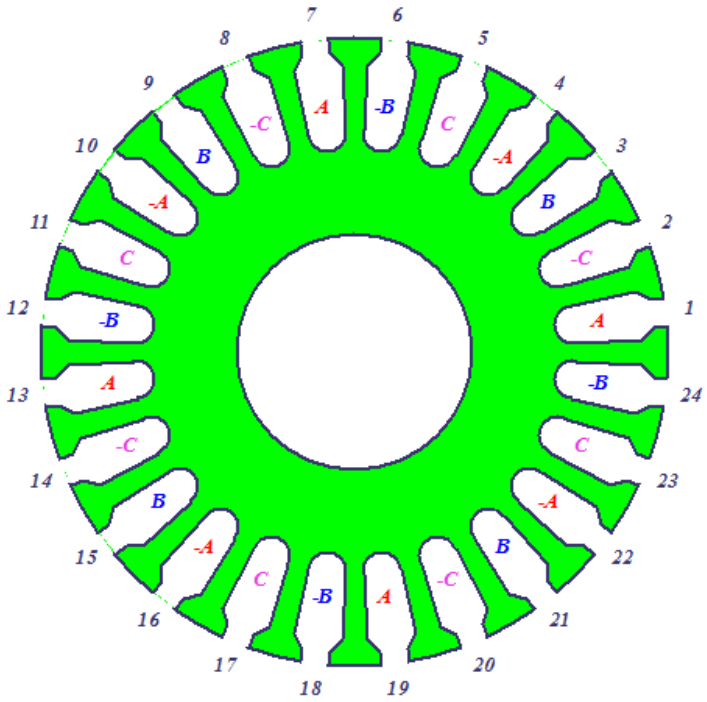

Figure 4.5. Winding layout of the designed PMSG

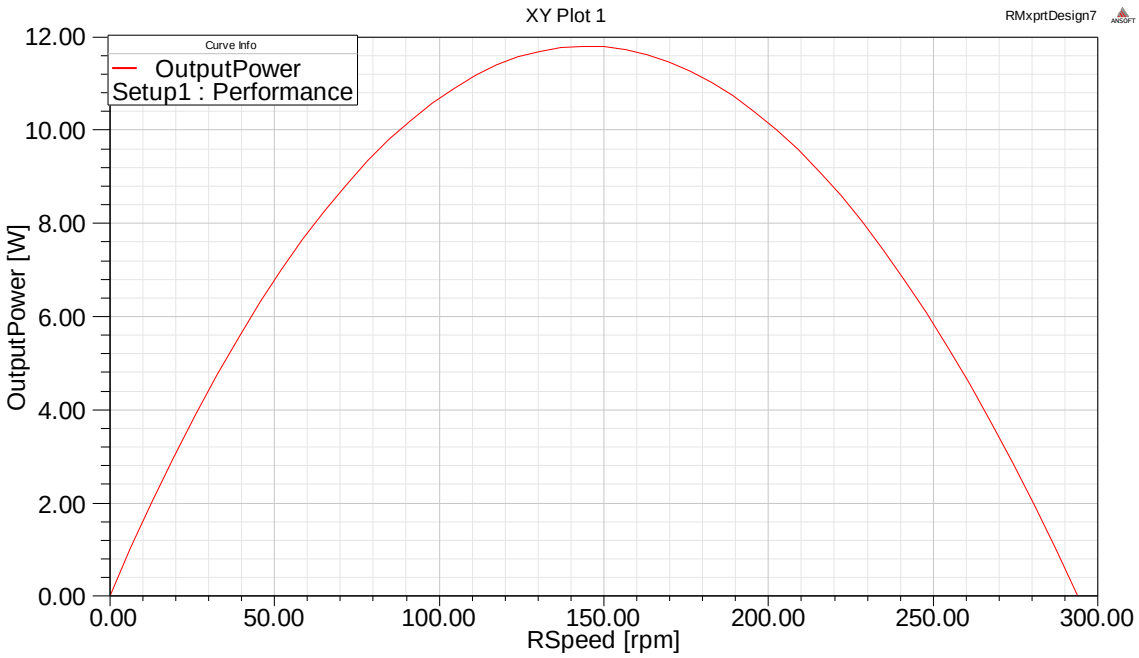

Figure 4.6. Output power vs. rotational speed

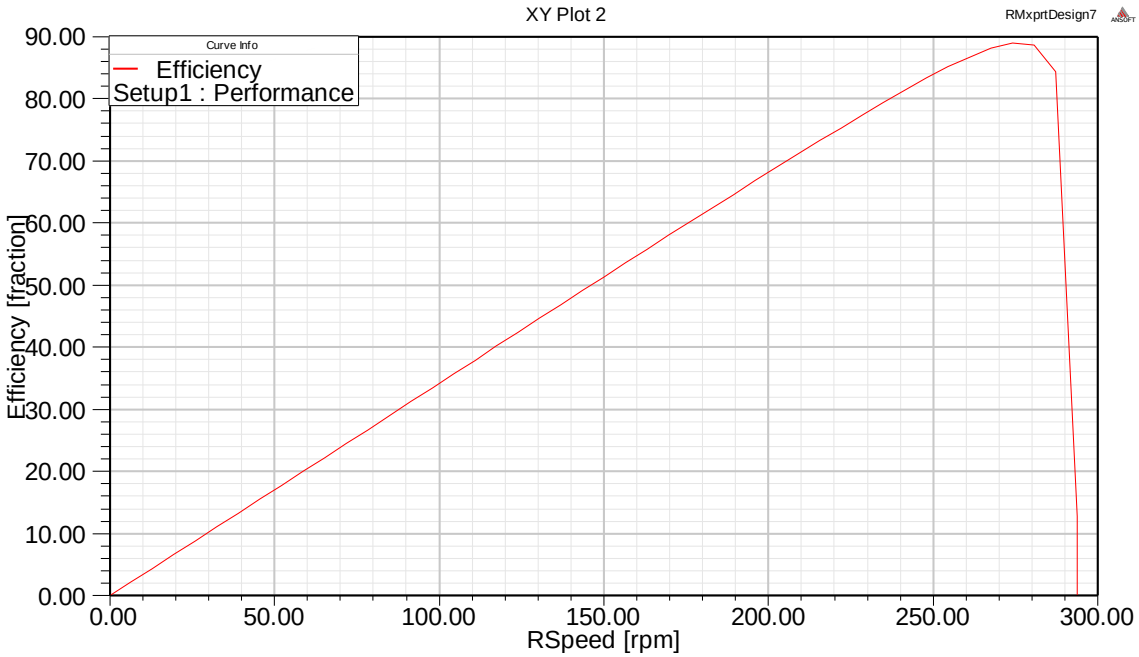

Figure 4.7. Efficiency vs. rotational speed

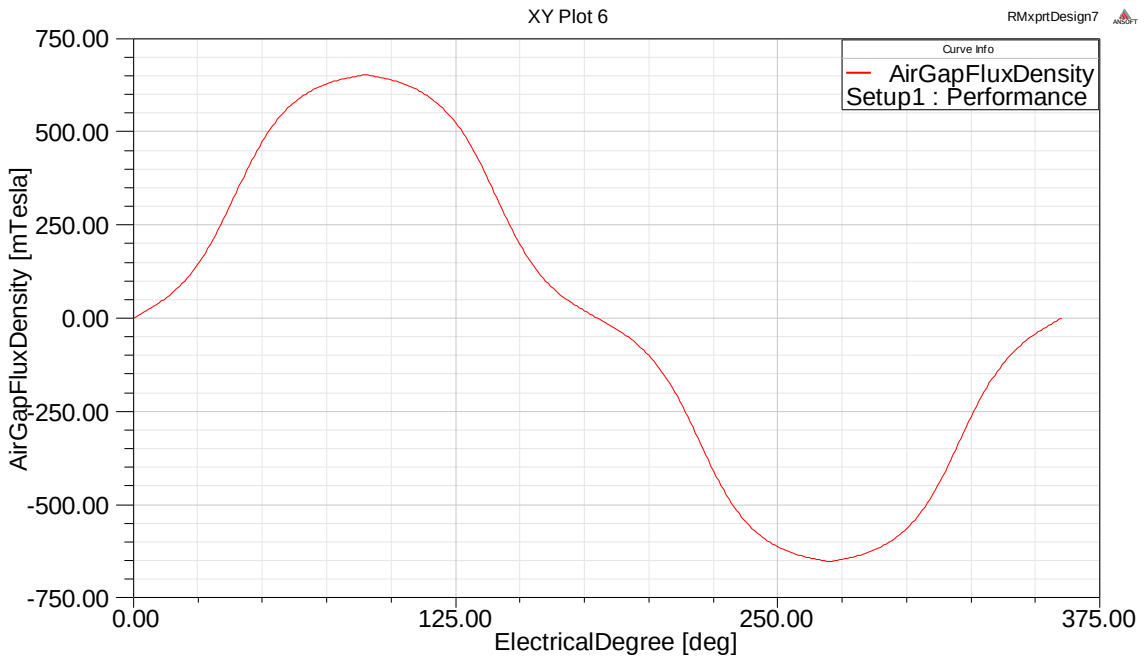

Figure 4.8. Air gap flux density

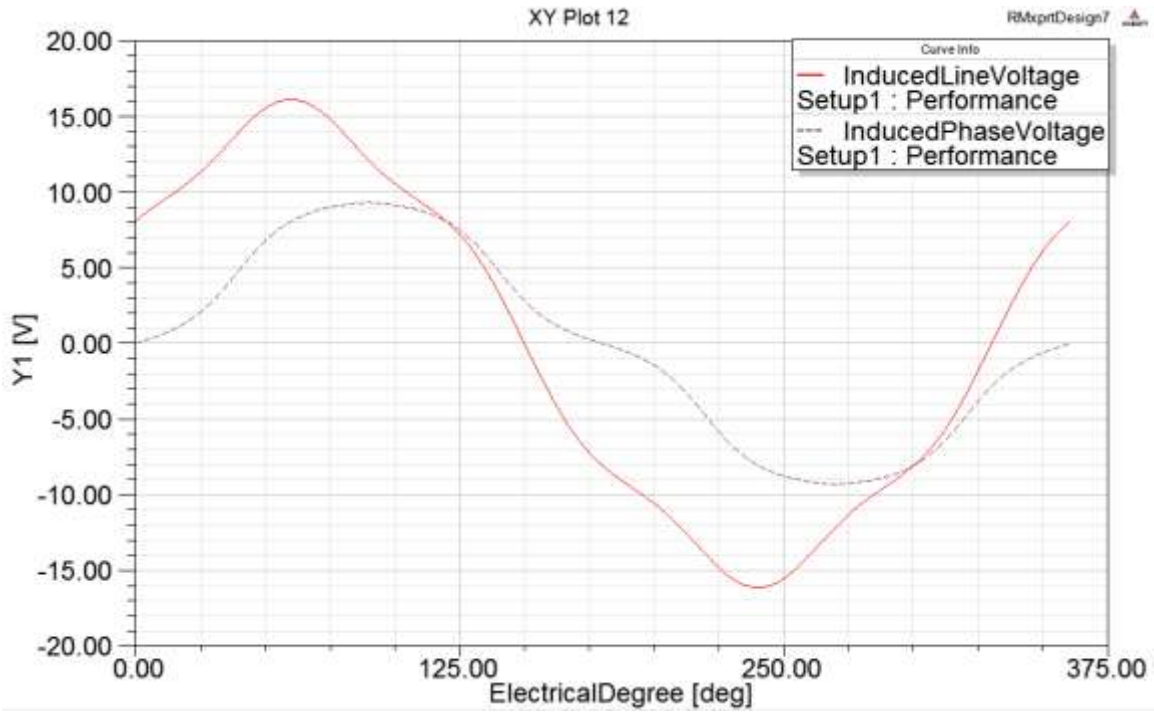

Figure 4.9. Induced phase and line voltage

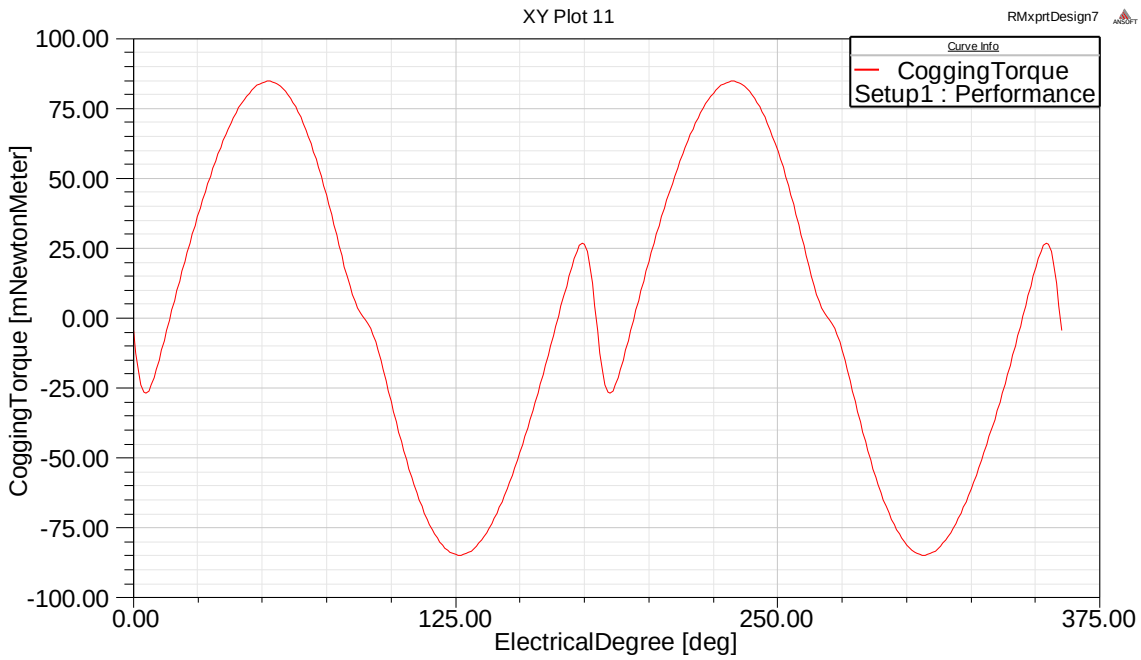

Figure 4.10. Cogging torque

The simulation results can be verified by the PMSG design equations. First of all, from the pole pitch τ_p and the width of the magnet τ_m, the magnet fraction can be calculated

$$\alpha_m = \frac{\tau_m}{\tau_p} \tag{21}$$

Air gap flux density B_g can be expressed as

$$B_g = \frac{C_\phi B_r}{1 + \mu_r k_c \frac{k_{ml}}{P_c}} \tag{22}$$

In order to calculate the air gap flux density B_g, flux concentration factor C_Φ, permeance coefficient P_c, magnet leakage factor k_{ml}, carter coefficient k_c and remanence B_r needs to be calculated

$$C_\phi = 2\frac{\alpha_m}{1+\alpha_m} \tag{23}$$

$$P_c = \frac{L_m}{gC_\phi} \tag{24}$$

$$k_c = \left[1 - \frac{1}{\frac{\tau_s}{W_s}\left(5\frac{g_c}{W_s}+1\right)}\right]^{-1} \tag{25}$$

$$k_{ml} = 1 + 4\frac{L_m \ln\left[1+\pi\frac{g}{(1-\alpha_m)\tau_p}\right]}{\pi\mu_r\alpha_m\tau_p} \tag{26}$$

$$B_r = H_c\mu_o\mu_r \tag{27}$$

Once the air gap flux density is obtained, the induced peak back EMF can be expressed as

$$E_{\max} = N_m B_g L R_{so} N_{spp} n_s \omega_m \tag{28}$$

where N_m is the number of magnets, B_g is the air gap flux density, L is the length of the stator, R_{so} is the stator outer radius, N_{spp} is the number of slots per pole per phase, n_s is the number of turns per slot and ω_m is the rotational speed of the generator.

After applying the parameters of the designed PMSG into the equations above, the peak back EMF is 7.09 V which is close to the simulation result 9.3 V. The difference of these two results may be caused by the approximation used in the equations above. Also, the distribution factor, pitch factor and the skew factor are not taken into account during the above calculations.

4.3.2. Magnetostatic Simulation in Maxwell 2D. Though RMxprt is able to simulate the performance of the designed PMSG in terms of output power, efficiency, induced voltage, and other dynamic performance, it does not give the magnetostatic properties of the designed PMSG. In order to simulate the magnetostatic properties such as flux distribution and flux density distribution of the designed PMSG in RXxprt, a finite element analysis (FEA) needs to be conducted. Therefore, a Maxwell 2D model

needs to be designed. Figure 4.11 shows the cross section view of the designed PMSG in Maxwell 2D. The parameters and dimensions of this PMSG is the same as the one designed using RMxprt. Figure 4.12 shows the flux distribution of the designed PMSG in Maxwell 2D. Figure 4.13 shows the flux density distribution of the designed PMSG in Maxwell 2D. The maximum flux density is 1.28 T and this high flux density only exists at the edge of the magnets where the flux paths through the outer steel part of the rotor. Therefore, this PMSG design does not have flux saturation issues.

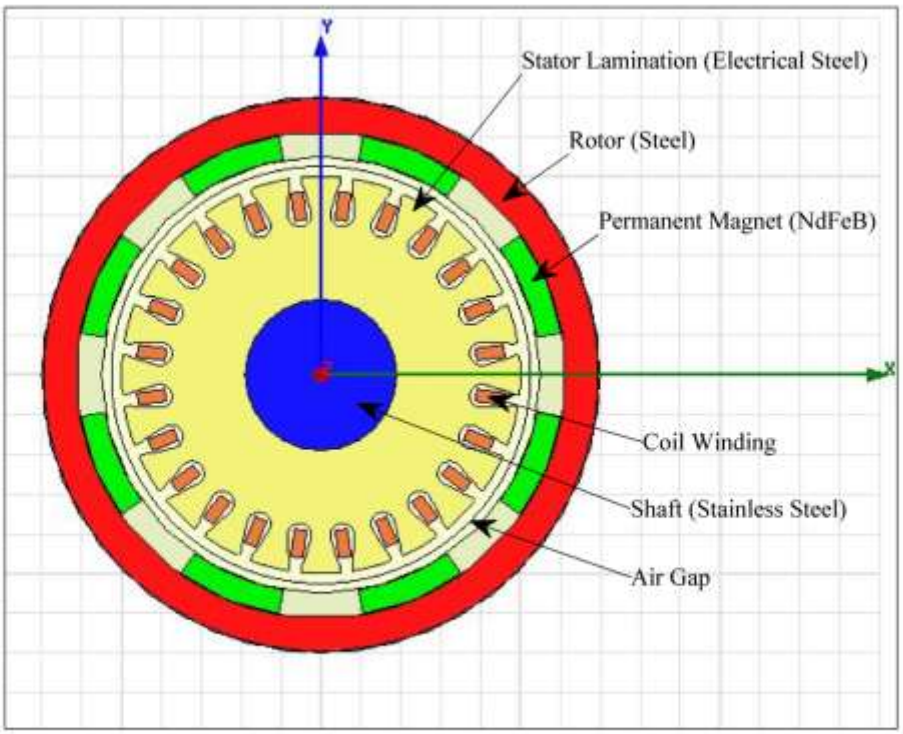

Figure 4.11. Cross section view of the designed PMSG in Maxwell 2D

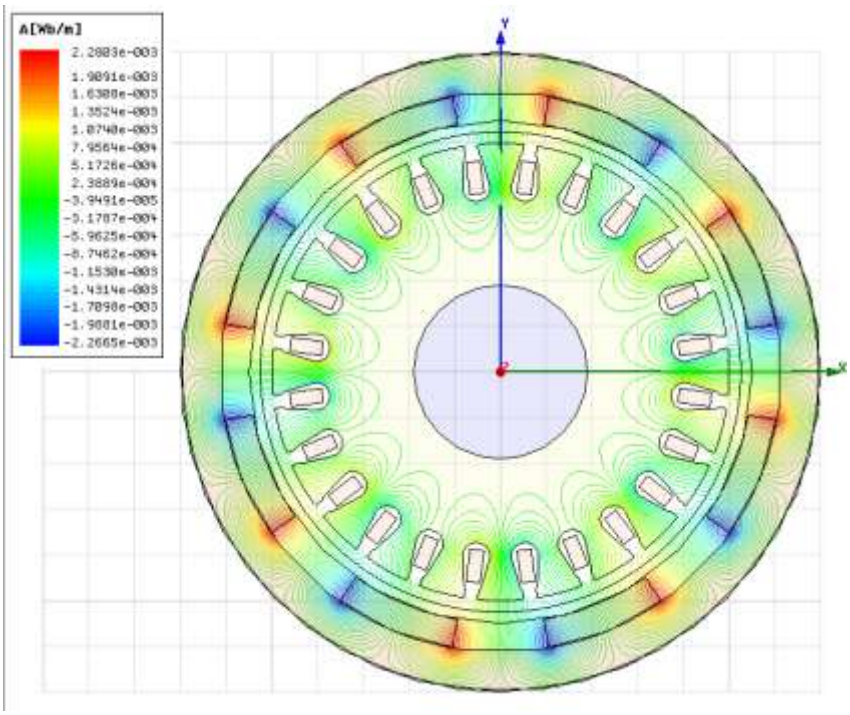

Figure 4.12. Flux line distribution of the designed PMSG in Maxwell 2D

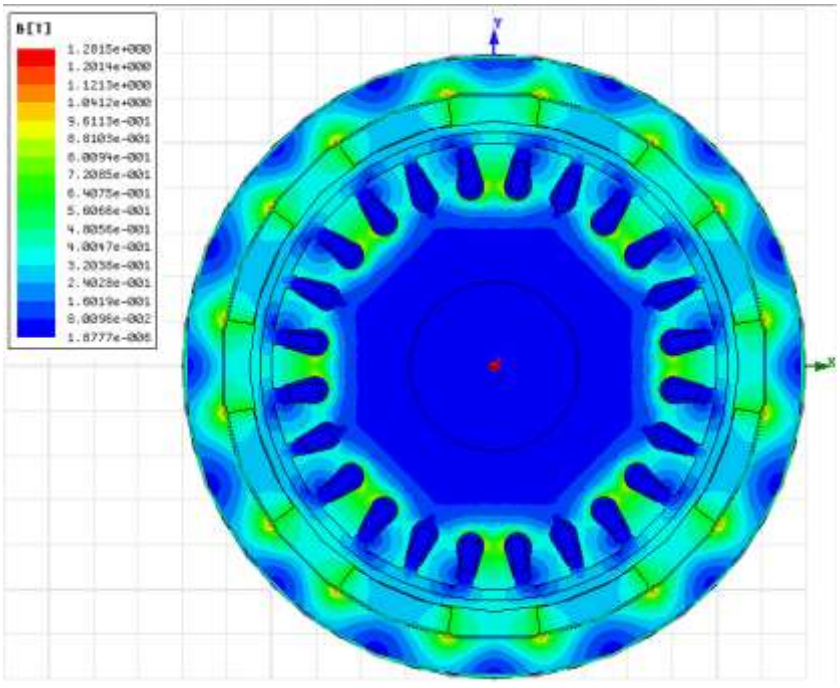

Figure 4.13. Flux density distribution of the designed PMSG in Maxwell 2D

4.4. TEST RESULTS

In order to test the performance of the designed PMSG, the physical motor is built as shown in Fig. 4.14. One of the most challenging difficulties encountered during construction of the motor is that the stator lamination pieces are very sharp and they tend to cut into the insulation layers of the magnetic wire causing multiple shorts among the different phases. In order to avoid this problem, additional insulation needs to be provided on the windings. In this case, electrical tape is used in the stator slots to provide the additional protection between the laminations and the windings. However the available space in the slots for windings is reduced. When the motor is finally constructed, there are only 10 turns per slot instead of the 35 turns per slot as designed previously. The actual phase inductance and phase resistance is measured which is 249 μH and 1.253 Ohms respectively.

Figure 4.14. PMSG built based on the RMxprt design

An induction motor is used to drive the PMSG to test its performance. Figure 4.15 (a)-Figure 4.22 (a) shows the experiment results of generated three phase voltages under

different rotational speed. Figure 4.15 (b)-Figure 4.22 (b) shows the simulation results of induced phase voltages under the corresponding rotational speed in experiment.

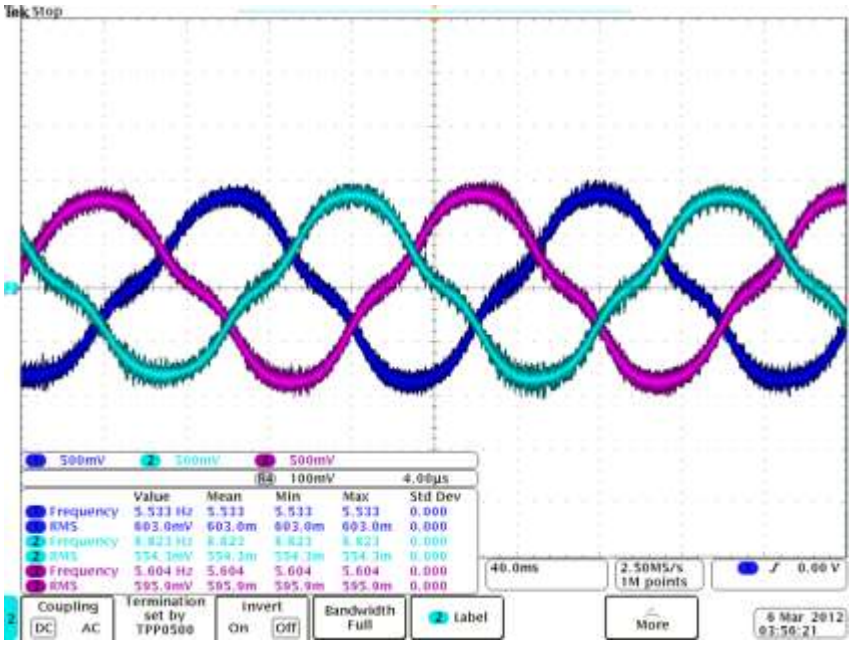

Figure 4.15 (a) Experimental result of three phase voltage at 84 rpm

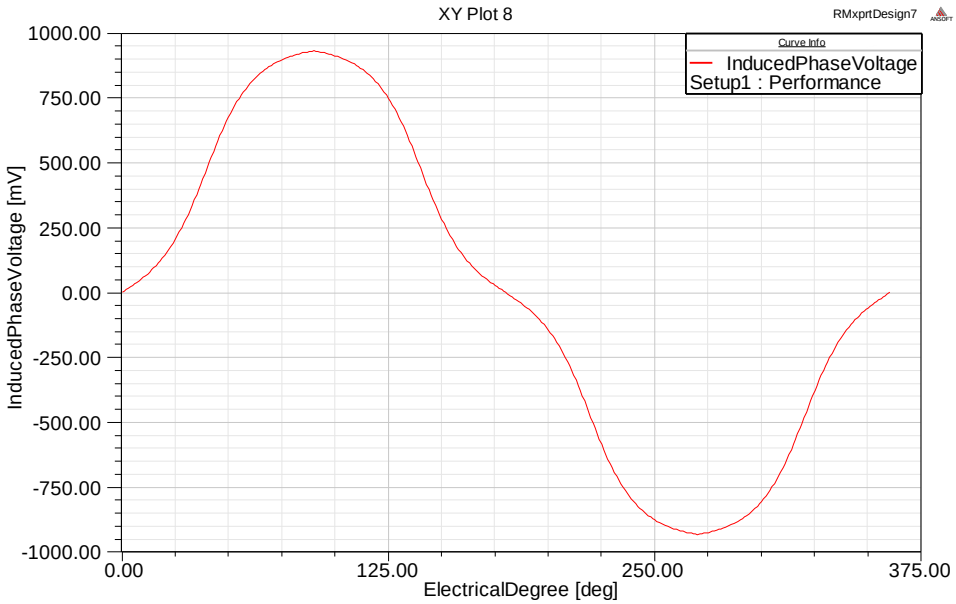

Figure 4.15 (b) Simulation result of induced phase voltage at 84 rpm

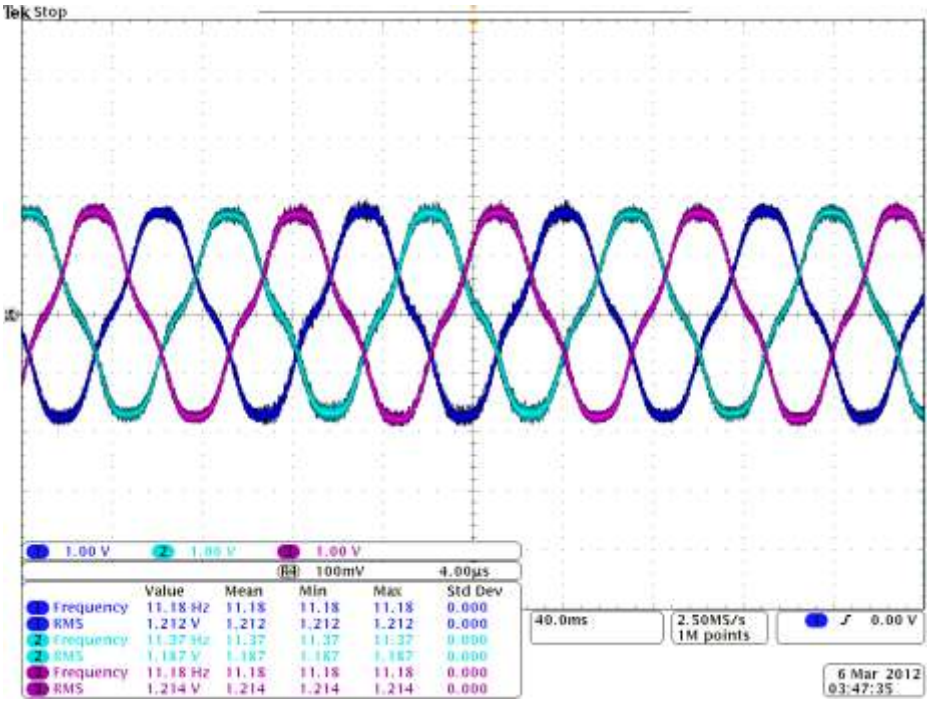

Figure 4.16 (a) Experimental result of three phase voltage at 171 rpm

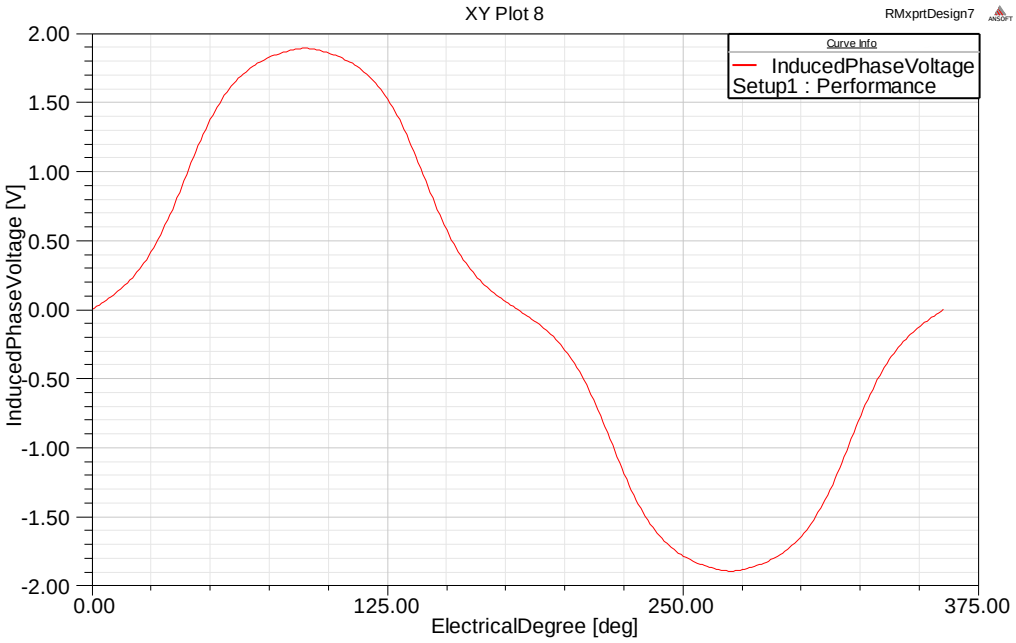

Figure 4.16 (b) Simulation result of three phase voltage at 171 rpm

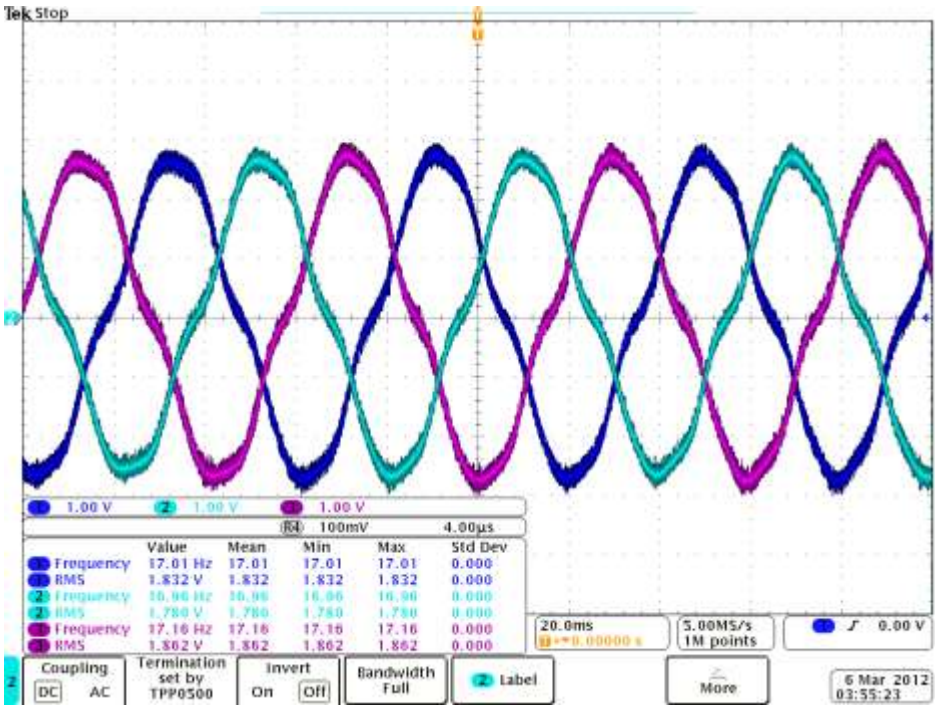

Figure 4.17 (a) Experimental result of three phase voltage at 258 rpm

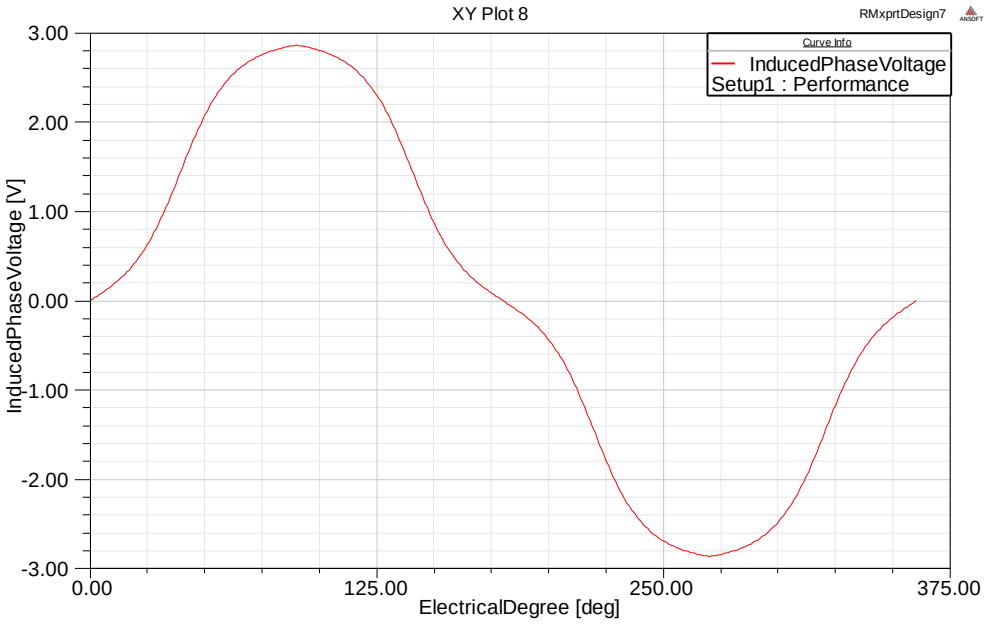

Figure 4.17 (b) Simulation result of three phase voltage at 258 rpm

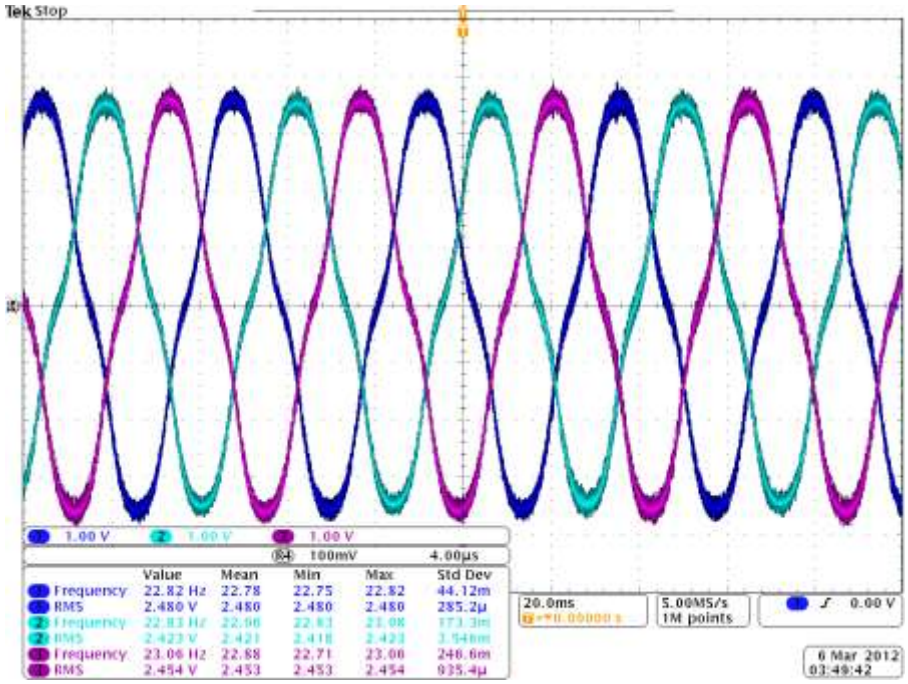

Figure 4.18 (a) Experimental result of three phase voltage at 345 rpm

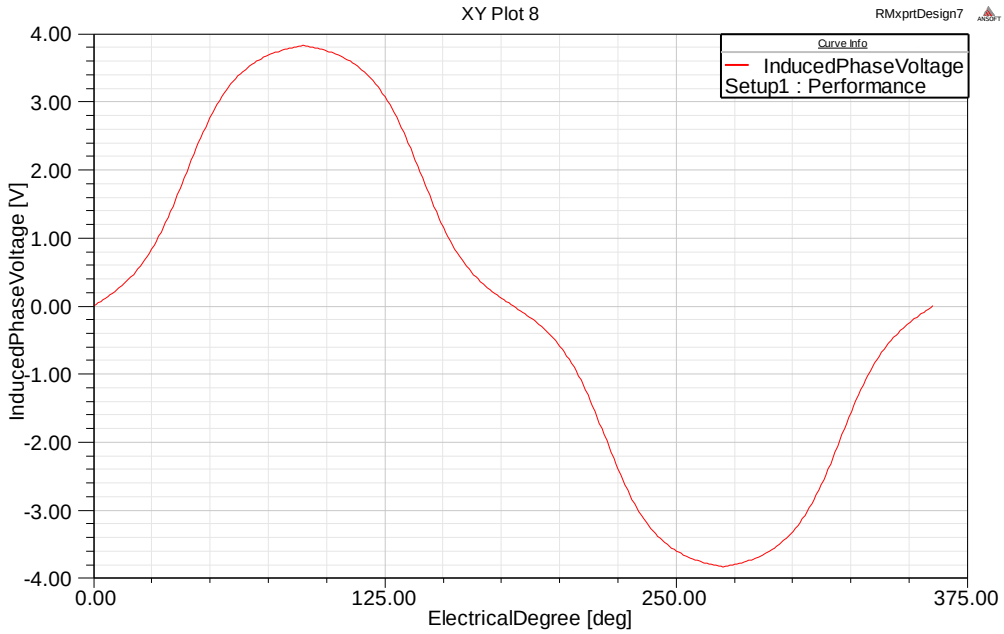

Figure 4.18 (b) Simulation result of three phase voltage at 345 rpm

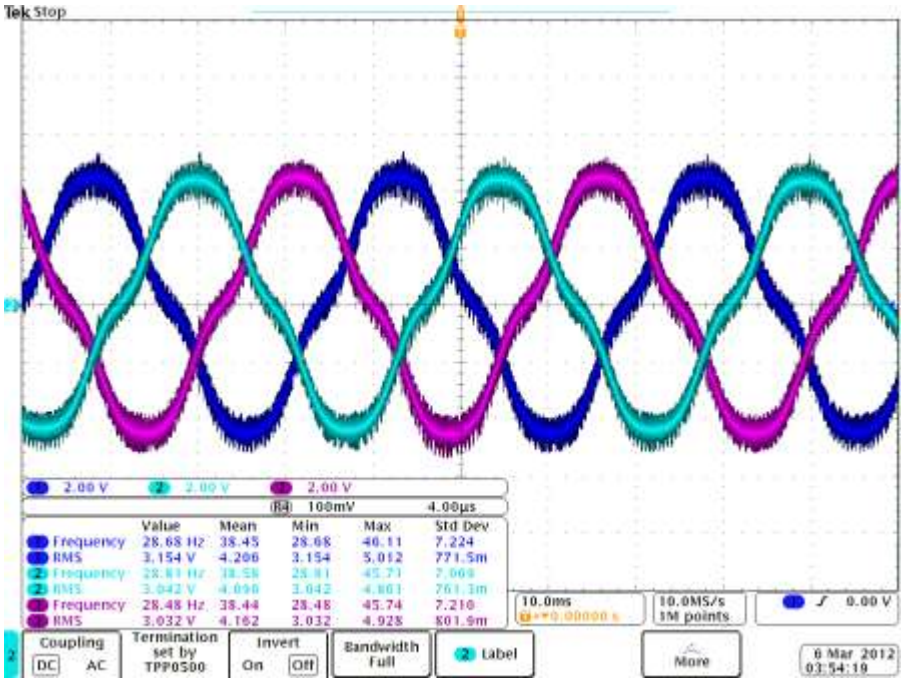

Figure 4.19 (a) Experimental result of three phase voltage at 432 rpm

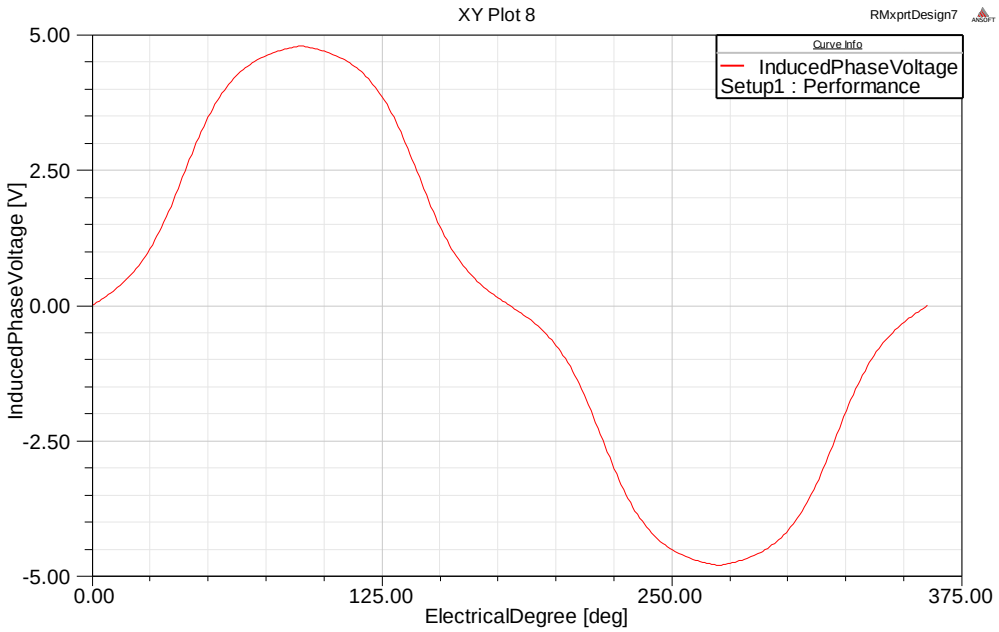

Figure 4.19 (b) Simulation result of three phase voltage at 432 rpm

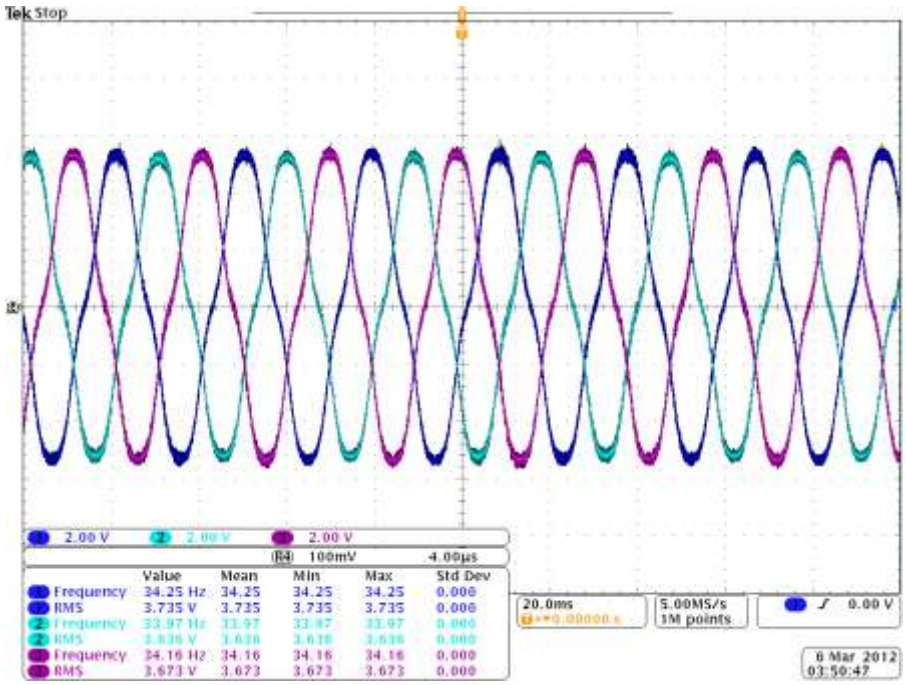

Figure 4.20 (a) Experimental result of three phase voltage at 519 rpm

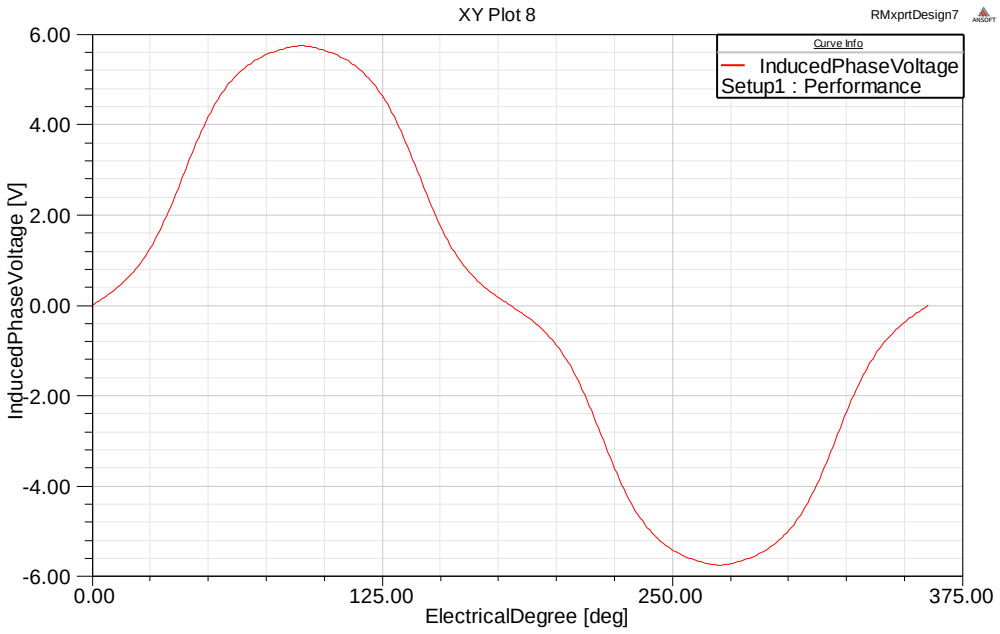

Figure 4.20 (b) Simulation result of three phase voltage at 519 rpm

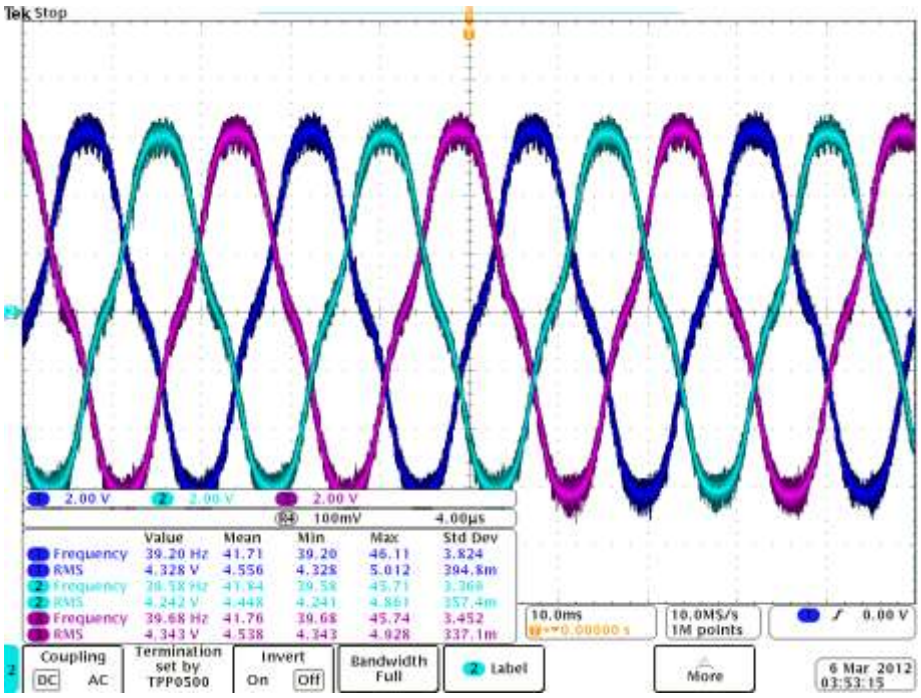

Figure 4.21 (a) Experimental result of three phase voltage at 606 rpm

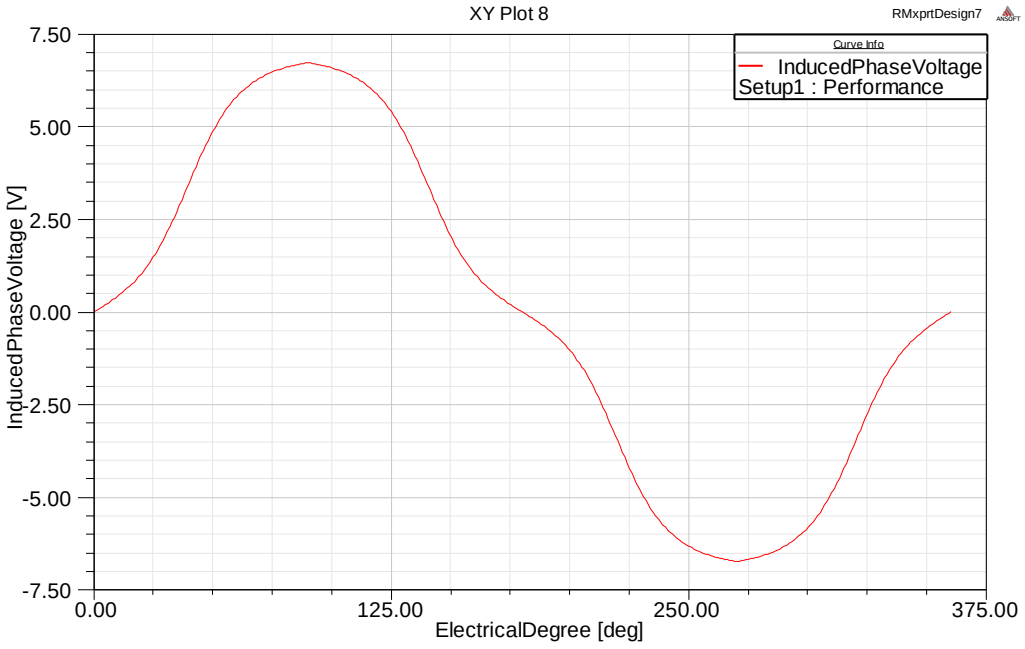

Figure 4.21 (b) Simulation result of three phase voltage at 606 rpm

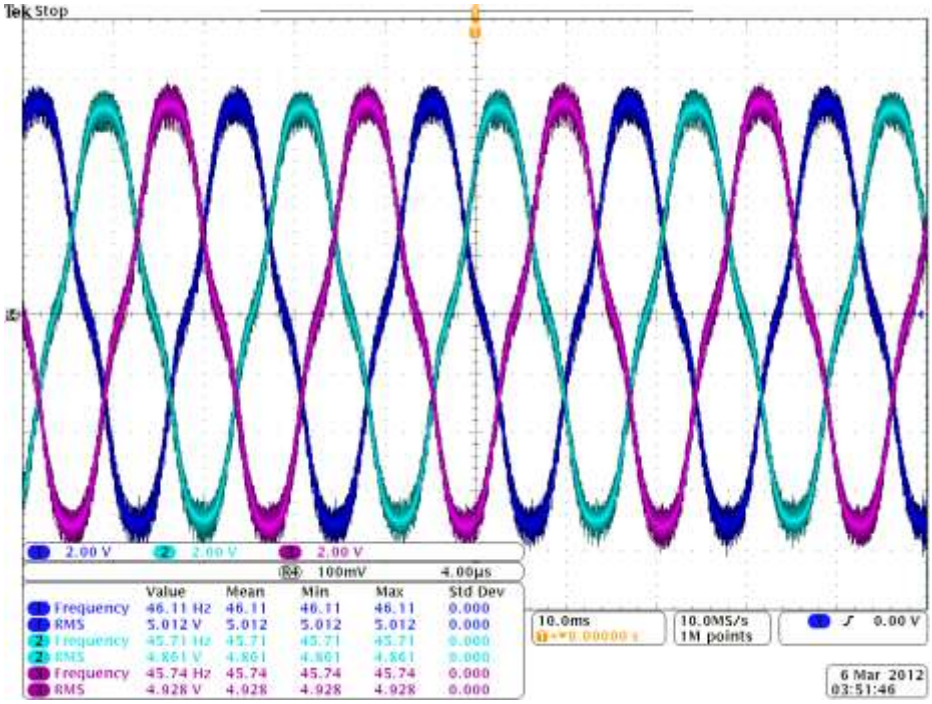

Figure 4.22 (a) Experimental result of three phase voltage at 693 rpm

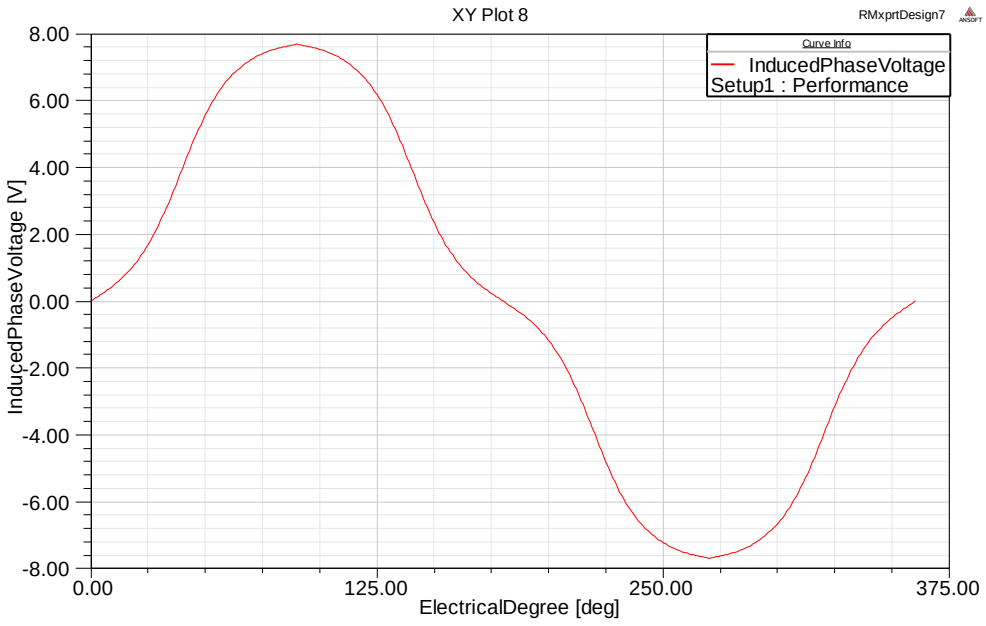

Figure 4.22 (b) Simulation result of three phase voltage at 693 rpm

Figure 4.15-Figure 4.22 shows that the experiment results of the generated phase voltage is the same as the simulation results in RMxprt. Table 4.2 shows the experimental results of the rms value of the induced phase voltage, back EMF constant, electrical frequency ω_e, mechanical frequency ω_m, and the ratio of ω_e over ω_m under different rotational speed. Since it's an 8 pole machine, the ratio of ω_e/ω_m should be the number of pole pairs which is 4. This is validated by the results shown in Table 4.2 where ω_e/ω_m is close to 4 under different rotational speed. Figure 4.23 shows the relationship between the rms value of the induced phase voltage and the rotational speed. Based on Figure 4.23, the rms value of the induced phase voltage and the rotational speed of the PMSG is almost a linear relationship and this relationship can be characterized by the parameter called back EMF constant. According to table 4.2, the back EMF constant of this machine is around 0.007 V/rpm.

Table 4.2. Test results of PMSG under different rotational speed

Speed (rpm)	Phase voltage rms (V)	BACK EMF V/rpm	ω_e	ω_m	ω_e/ω_m
84	0.584415827	0.006957331	5.55	1.4	3.96905
171	1.204479561	0.00704374	11.24	2.85	3.94503
258	1.82442574	0.007071418	17.04	4.3	3.96357
345	2.45248916	0.007108664	22.9	5.75	3.98319
432	3.076042872	0.00712047	28.65	7.2	3.98009
519	3.681418494	0.007093292	34.12	8.65	3.94528
606	4.304191447	0.007102626	39.48	10.1	3.90957
693	4.933487348	0.007119029	45.85	11.55	3.96999

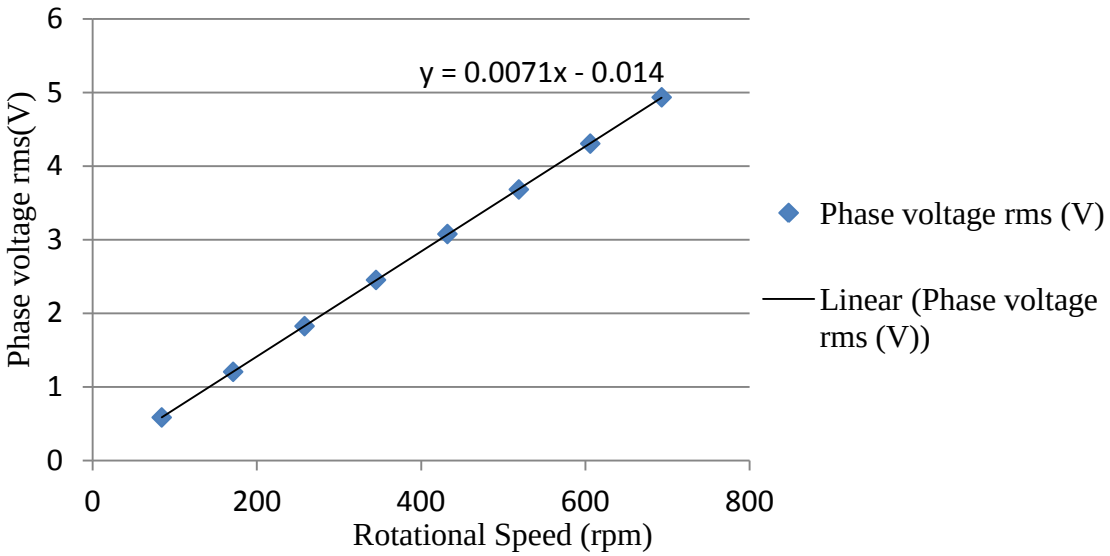

Figure 4.23 Experiment results of phase voltage vs. rotational speed

5. CONCLUSIONS AND FUTURE WORK

5.1. CONCLUSION

River-based hydrokinetic turbine system is studied and discussed in terms of system level design and power flow control method in this thesis. Hydrokinetic turbine power characteristics is also analyzed and its similar capability of variable speed operation for maximum power extraction has led to the proposal of maximum power point tracking (MPPT) control for hydrokinetic turbines.

A complete mathematical model of the hydrokinetic system is developed. This model analyzes the interaction between the mechanical part of the system and the electrical part of the system. Based on the developed model of the hydrokinetic turbine system, a boost converter is used to implement the proposed MPPT control. The developed MPPT control is similar to the hill-climbing method used as MPPT control in photovoltaic systems. In addition, the proposed MPPT control strategy is generic to all the hydrokinetic turbine systems. Simulation and experiment results validate the performance of the proposed control strategy.

In order to improve the efficiency of the power transmission of the hydrokinetic system, a low-speed high-thrust permanent magnet synchronous generator (PMSG) is recommended for the small scale stand-alone hydrokinetic turbine systems. The adoption of a low-speed high-thrust generator can eliminate the use of a speed increaser, thus reducing the transmission power losses imposed by the speed increaser. A low-speed high-thrust PMSG is also designed for the hydrokinetic turbine system using RMxprt. A Maxwell 2D model of the designed PMSG is also developed to simulate the magnetostatic performance of the machine. A physical prototype of the designed PMSG is built and tested as well.

5.2. FUTURE WORK

River-based hydrokinetic turbine system is still at its elementary stage in terms of commercialization. There are still a lot to be done. In terms of structure, a new design is necessary for the integration of the hydrokinetic turbine and the electrical system such as the PMSG and the power converters. In terms of electrical part for the system, grid

interface can be developed so that the extra amount of potential power from the hydrokinetic turbine can be injected into the grid, saving the customers money and making the hydrokinetic turbine system more cost-effective. In addition, the system can be scaled up so that it has more power capability.

APPENDIX A.
PRINTED CIRCUIT BOARD DESIGN

This appendix includes the schematic and board layout of the printed circuit board described in Section 3.6. The schematic diagram is shown in Figure A.1. The physical board layout pictured in Figure 3.17, is broken into two parts to show the top and the bottom layers of the board separately. The board layout for the top layer is shown in Figure A.2 and the board layout for the bottom layer is shown in Figure A.3.

.

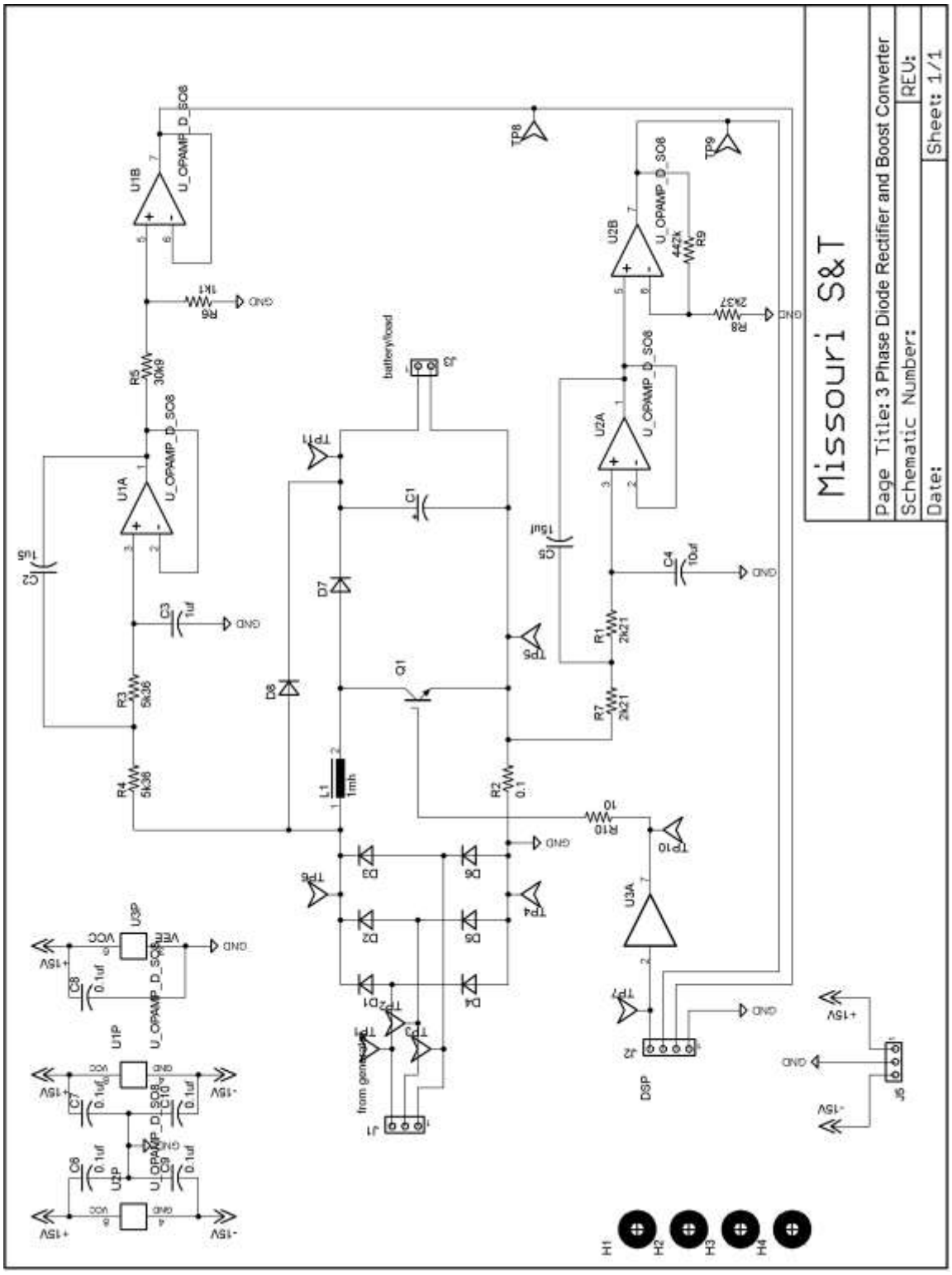

Figure A.1. Printed circuit board schematic

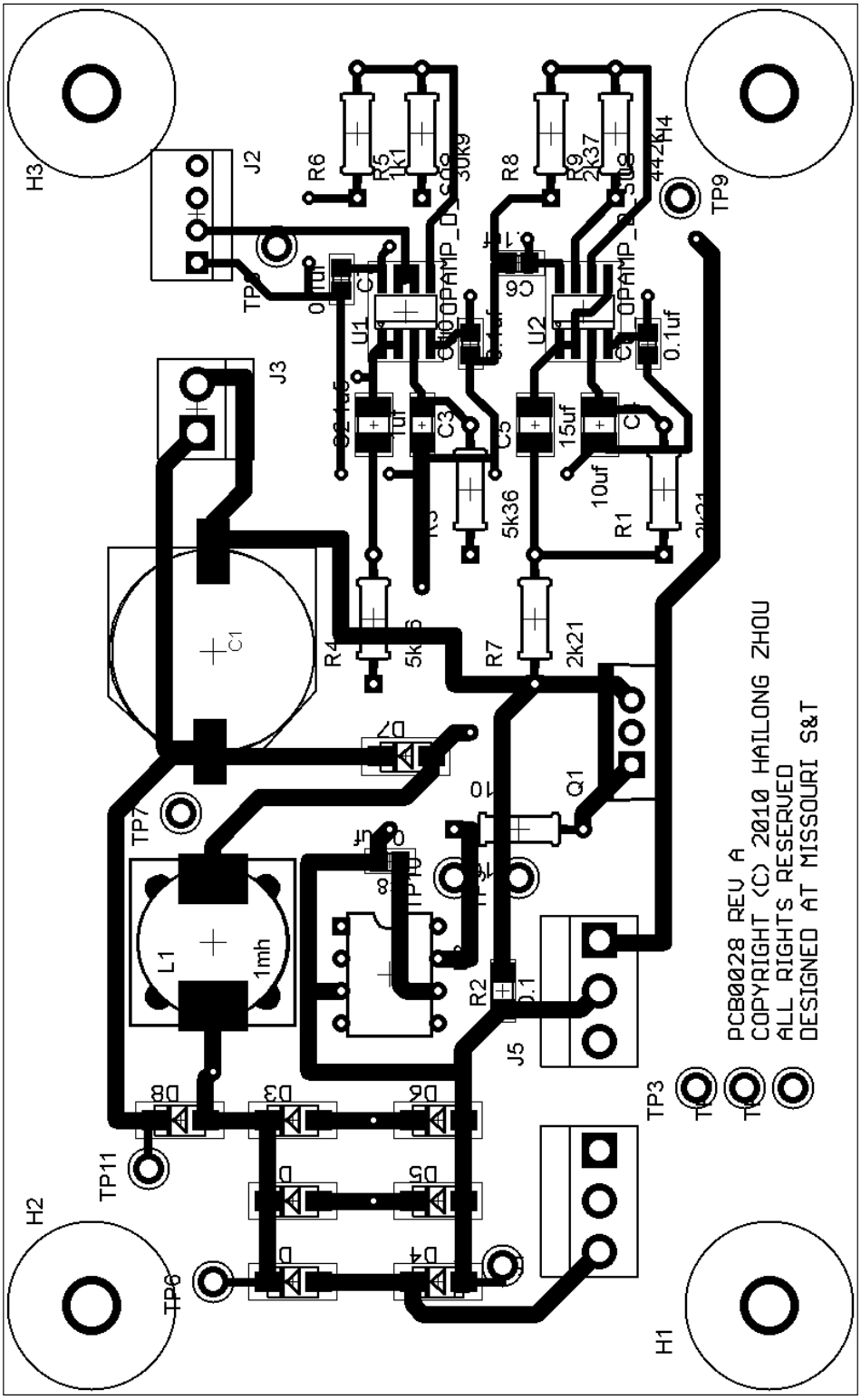

Figure A.2. Physical board layout of top layer

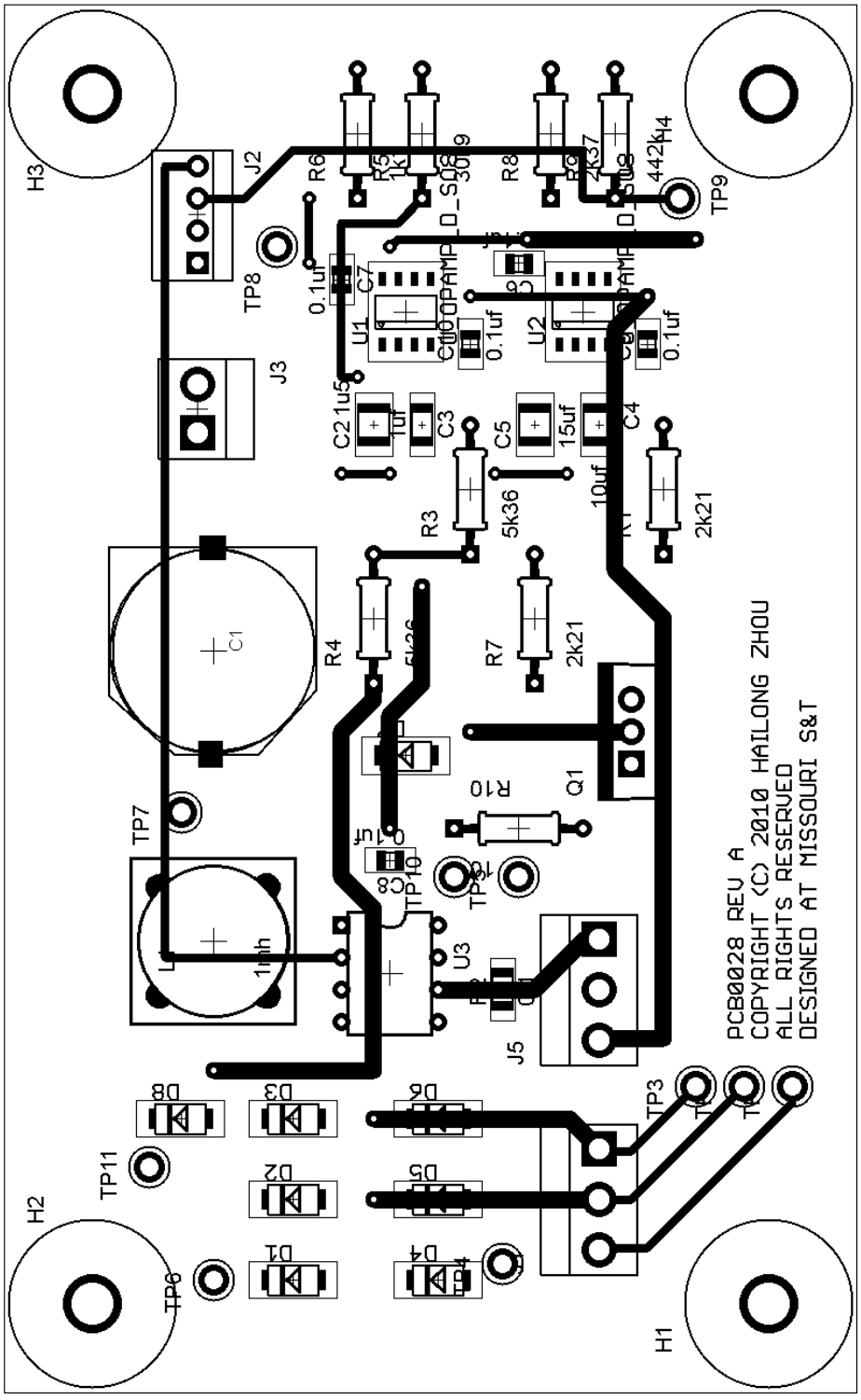

Figure A.3. Physical board layout of bottom layer

APPENDIX B.
DSP CODE FOR THE PROPOSED MPPT CONTROL ALGORITHM

This appendix includes the C code of the proposed MPPT algorithm programmed into the DSP28335 microcontroller. There are detailed comments of explanation for each block of codes. The comments are denoted by text which is preceded with two forward slash symbols (//).

```
// Copyright by Hailong Zhou
// All Rights Reserved
// MPPT Control Algorithm for Hydrokinetic Turbine
//###########################################################################
// Code Description:
//      This code is used to implement the MPPT control in the boost converter
// for the hydrokinetic turbine system. V_decimal and I_decimal is the
// measured voltage and current. These two are updated every 0.01 ms. However,
// the power P_now is updated every 0.1 s. The duty ratio is changed by varing
// the value of EPwm1Regs.CMPA.half.CMPA. The MPPT control and the speed
// sensing is realized in the interrupt service of timer0.
//###########################################################################

//###########################################################################
#include "DSP2833x_Device.h"

// External function prototypes
extern void InitAdc(void);
extern void InitSysCtrl(void);
extern void InitPieCtrl(void);
extern void InitPieVectTable(void);
extern void InitCpuTimers(void);
extern void ConfigCpuTimer(struct CPUTIMER_VARS *, float, float);

// Prototype statements for functions found within this file.
void Gpio_select(void);
void Setup_ePWM1A(void);
void Setup_ePWM2(void);
void Setup_ADC(void);
interrupt void cpu_timer0_isr(void);     //CPU TIMER0
interrupt void adc_isr(void);            // ADC  End of Sequence ISR

//Global variable.
int count = 0;
int start_up = 1;
int up = 0;
float P_now = 0;
float P_before = 0;
unsigned int Voltage_V;
unsigned int Voltage_I;
unsigned int Vg;
float V_decimal = 0;
float I_decimal = 0;
float P_decimal_now = 0;
float P_decimal_before = 0;
float Duty_ratio = 0;
float Dnumber = 0;
float pi = 3.141592653;
float T1 = 0;
float state_now = 0;
float state_before = 0;
```

```
float fe = 0;
float We = 0;
float Werpm = 0;
float Wm = 0;
float Wmrpm = 0;
float pulse_count = 0;
float Torque = 0;
float Rps = 0;

//###########################################################################
//                                       main code
//###########################################################################
void main(void)
{
       InitSysCtrl();             // Basic Core Init from DSP2833x_SysCtrl.c

       EALLOW;
       SysCtrlRegs.WDCR= 0x00AF;  // Re-enable the watchdog
       EDIS;               // 0x00AF to NOT disable the Watchdog, Prescaler = 64

       DINT;                      // Disable all interrupts

       Gpio_select();             // GPIO set up

       Setup_ePWM1A();            // Init of ePWM1A

       InitPieCtrl();     // Basic setup of PIE table; from DSP2833x_PieCtrl.c

       InitPieVectTable();       // Default ISR's in PIE

       Setup_ADC();               // Init of ADC

       Setup_ePWM2();             // Init of ePWM2

       EALLOW;
       PieVectTable.TINT0 = &cpu_timer0_isr;
       PieVectTable.ADCINT = &adc_isr;
       EDIS;

       InitCpuTimers();           // Basic setup CPU Timer0, 1 and 2

       ConfigCpuTimer(&CpuTimer0,150,10);  // Timer configuration, 0.01ms

       PieCtrlRegs.PIEIER1.bit.INTx6 = 1;          // ADC
       PieCtrlRegs.PIEIER1.bit.INTx7 = 1;        // CPU Timer

       IER |=1;

       EINT;
       ERTM;

       CpuTimer0Regs.TCR.bit.TSS = 0;    // Start timer0

       while(1)
       {
              EALLOW;
              SysCtrlRegs.WDKEY = 0x55;  // Service WD #1
              EDIS;
       }
}

void Gpio_select(void)    // GPIO set up
{
```

```
       EALLOW;
       GpioCtrlRegs.GPAMUX1.all = 0;           // GPIO15 ... GPIO0 = General
Puropse I/O
       GpioCtrlRegs.GPAMUX1.bit.GPIO0 = 1;     // ePWM1A active

       GpioCtrlRegs.GPAMUX2.all = 0;           // GPIO31 ... GPIO16 = General
Purpose I/O
       GpioCtrlRegs.GPBMUX1.all = 0;           // GPIO47 ... GPIO32 = General
Purpose I/O
       GpioCtrlRegs.GPBMUX2.all = 0;           // GPIO63 ... GPIO48 = General
Purpose I/O
       GpioCtrlRegs.GPCMUX1.all = 0;           // GPIO79 ... GPIO64 = General
Purpose I/O
       GpioCtrlRegs.GPCMUX2.all = 0;           // GPIO87 ... GPIO80 = General
Purpose I/O

       GpioCtrlRegs.GPADIR.all = 0;
       GpioCtrlRegs.GPADIR.bit.GPIO0 = 1;       // GPIO0 as output PWM
        GpioCtrlRegs.GPBDIR.all = 0;            // GPIO63-32 as inputs
       GpioCtrlRegs.GPCDIR.all = 0;             // GPIO87-64 as inputs
       EDIS;
}

void Setup_ePWM1A(void)                         //Set up ePWM1A 100K
{
       EPwm1Regs.TBCTL.bit.CLKDIV = 0;          // CLKDIV = 1
       EPwm1Regs.TBCTL.bit.HSPCLKDIV = 0;       // HSPCLKDIV = 2
       EPwm1Regs.TBCTL.bit.CTRMODE = 2;         // up - down mode

       EPwm1Regs.AQCTLA.all = 0x0060;           // Set ePWM1A on CMPA up
                                                // Clear ePWM1A on CMPA down

       EPwm1Regs.TBPRD = 750;                   // 100KHz - PWM signal
       EPwm1Regs.CMPA.half.CMPA = 750;          // 0% duty cycle first
}

void Setup_ePWM2(void)                          //Set up ePWM2 100K
{
       EPwm2Regs.TBCTL.all = 0xC030;    // Configure timer control register
       /*
        bit 15-14     11:     FREE/SOFT, 11 = ignore emulation suspend
        bit 13        0:      PHSDIR, 0 = count down after sync event
        bit 12-10     000:    CLKDIV, 000 => TBCLK = HSPCLK/1
        bit 9-7       000:    HSPCLKDIV, 000 => HSPCLK = SYSCLKOUT/1
        bit 6         0:      SWFSYNC, 0 = no software sync produced
        bit 5-4       11:     SYNCOSEL, 11 = sync-out disabled
        bit 3         0:      PRDLD, 0 = reload PRD on counter=0
        bit 2         0:      PHSEN, 0 = phase control disabled
        bit 1-0       00:     CTRMODE, 00 = count up mode
       */

       EPwm2Regs.TBPRD = 2999;    // TBPRD +1  =  TPWM / (HSPCLKDIV * CLKDIV *
TSYSCLK)
                                  //           =  20 M / 6.667 ns
                                  //100K

       EPwm2Regs.ETPS.all = 0x0100;     // Configure ADC start by ePWM2
       /*
        bit 15-14     00:     EPWMxSOCB, read-only
        bit 13-12     00:     SOCBPRD, don't care
        bit 11-10     00:     EPWMxSOCA, read-only
        bit 9-8       01:     SOCAPRD, 01 = generate SOCA on first event
        bit 7-4       0000:   reserved
```

```
        bit 3-2        00:     INTCNT, don't care
        bit 1-0        00:     INTPRD, don't care
       */

       EPwm2Regs.CMPA.half.CMPA = 15000;             // 0% duty cycle first

       EPwm2Regs.ETSEL.all = 0x0A00;           // Enable SOCA to ADC
       /*
        bit 15         0:      SOCBEN, 0 = disable SOCB
        bit 14-12      000:    SOCBSEL, don't care
        bit 11         1:      SOCAEN, 1 = enable SOCA
        bit 10-8       010:    SOCASEL, 010 = SOCA on PRD event
        bit 7-4        0000:   reserved
        bit 3          0:      INTEN, 0 = disable interrupt
        bit 2-0        000:    INTSEL, don't care
       */
}

void Setup_ADC(void)
{
       InitAdc();                 // Basic ADC setup, incl. calibration

       AdcRegs.ADCTRL1.all = 0;
       AdcRegs.ADCTRL1.bit.ACQ_PS = 7;          // 7 = 8 x ADCCLK
       AdcRegs.ADCTRL1.bit.SEQ_CASC = 1;        // 1=cascaded sequencer
       AdcRegs.ADCTRL1.bit.CPS = 0;             // divide by 1
       AdcRegs.ADCTRL1.bit.CONT_RUN = 0;        // single run mode

       AdcRegs.ADCTRL2.all = 0;
       AdcRegs.ADCTRL2.bit.INT_ENA_SEQ1 = 1;    // 1=enable SEQ1 interrupt
       AdcRegs.ADCTRL2.bit.EPWM_SOCA_SEQ1 = 1; // 1=SEQ1 start from ePWM_SOCA
trigger
       AdcRegs.ADCTRL2.bit.INT_MOD_SEQ1 = 0;    // 0= interrupt after every end
of sequence

       AdcRegs.ADCTRL3.bit.ADCCLKPS = 3;// ADC clock: FCLK = HSPCLK / 2 *
ADCCLKPS
                                        // HSPCLK = 75MHz (see
DSP2833x_SysCtrl.c)
                                        // FCLK = 12.5 MHz

       AdcRegs.ADCMAXCONV.all = 3;      // 3 conversions from Sequencer 1

       AdcRegs.ADCCHSELSEQ1.bit.CONV00 = 0; // Setup ADCINA0 as 1st SEQ1 conv.
       AdcRegs.ADCCHSELSEQ1.bit.CONV01 = 1; // Setup ADCINA1 as 2nd SEQ1 conv.
       AdcRegs.ADCCHSELSEQ1.bit.CONV02 = 2; // Setup ADCINA2 as 3rd SEQ1 conv.
}

interrupt void cpu_timer0_isr(void)
{
       CpuTimer0.InterruptCount++;
       count++;
       EALLOW;
       SysCtrlRegs.WDKEY = 0xAA;  // Service WD #2
       EDIS;
//###########################################################################
// MPPT control
//###########################################################################
       if(start_up)
       {
              if(EPwm1Regs.CMPA.half.CMPA >300)
              {
                     if(CpuTimer0.InterruptCount%500==0)
```

```
                {
                        EPwm1Regs.CMPA.half.CMPA = EPwm1Regs.CMPA.half.CMPA-1;
                }
            }
            else
            {
                start_up = 0;
                up = 1;
            }
        }
        else
        {
            if(count%10000==0)
            {
                switch(up)
                {
                     case 1:
                     P_now = (Voltage_V/10)*(Voltage_I/10);
                     P_decimal_now = V_decimal*I_decimal;
                    if(P_decimal_now>P_decimal_before)
                    {
                       P_decimal_before = P_decimal_now;
                       EPwm1Regs.CMPA.half.CMPA = EPwm1Regs.CMPA.half.CMPA+10;
                    }
                    else
                    {
                       P_decimal_before = P_decimal_now;
                       EPwm1Regs.CMPA.half.CMPA = EPwm1Regs.CMPA.half.CMPA-10;
                           up = 0;
                    }
                    break;

                    case 0:
                       P_decimal_now = V_decimal*I_decimal;
                    if(P_decimal_now>P_decimal_before)
                    {
                       P_decimal_before = P_decimal_now;
                       EPwm1Regs.CMPA.half.CMPA = EPwm1Regs.CMPA.half.CMPA-10;
                    }
                    else
                    {
                       P_decimal_before = P_decimal_now;
                       EPwm1Regs.CMPA.half.CMPA = EPwm1Regs.CMPA.half.CMPA+10;
                       up = 1;
                    }
                    break;
                }
                count = 0;
            }
        }
//###########################################################################
// Speed sensing of the generator
//###########################################################################
        state_now = GpioDataRegs.GPADAT.bit.GPIO9;

        T1 = T1+0.00001;

        if((state_before==0)&&(state_now==1))
        {
            pulse_count = pulse_count+1;
            if(pulse_count==1000)
            {
                fe = pulse_count/T1;
```

```
                Rps = fe/400;
                Werpm = Rps*60;
                Wmrpm = Werpm/2;
                Wm = Wmrpm*2*pi/60;
                Torque = P_decimal_now/Wm;
                T1 = 0;
                pulse_count = 0;
            }
        }

        state_before = state_now;

        Dnumber = EPwm1Regs.CMPA.half.CMPA;
        Duty_ratio = Dnumber/750;

        PieCtrlRegs.PIEACK.all = PIEACK_GROUP1;
}


interrupt void  adc_isr(void)
{
        Voltage_V = AdcMirror.ADCRESULT0; // Voltage measurement
        Voltage_I = AdcMirror.ADCRESULT1;   // Current measurement
        V_decimal = Voltage_V*0.0212688;    // Voltage value in decimal
        I_decimal = Voltage_I*0.00012152;   // Current value in decimal
        // Reinitialize for next ADC sequence
        AdcRegs.ADCTRL2.bit.RST_SEQ1 = 1;       // Reset SEQ1
        AdcRegs.ADCST.bit.INT_SEQ1_CLR = 1;            // Clear INT SEQ1 bit
        PieCtrlRegs.PIEACK.all = PIEACK_GROUP1; // Acknowledge interrupt to PIE
}
//===========================================================================
// End of Code.
//===========================================================================
```

BIBLIOGRAPHY

[1] V. J. Ginter and J. K. Pieper, "Robust gain scheduled control of a hydrokinetic turbine part 1: Design," in *Proc. Electrical Power & Energy Conference (EPEC), 2009 IEEE*, 2009, pp. 1-6.

[2] D. Fujin and C. Zhe, "Power control of permanent magnet generator based variable speed wind turbines," in *Proc. Electrical Machines and Systems, 2009. ICEMS 2009. International Conference on*, 2009, pp. 1-6.

[3] D. Jinxu and A. Somani, "A Long-Term Investment Planning Model for Mixed Energy Infrastructure Integrated with Renewable Energy," in *Proc. Green Technologies Conference, 2010 IEEE*, 2010, pp. 1-10.

[4] S. Breban, B. Robyns, and M. M. Radulescu, "Study of a grid-connected hybrid wind/micro-hydro power system associated with a supercapacitor energy storage device," in *Proc. Optimization of Electrical and Electronic Equipment (OPTIM), 2010 12th International Conference on*, 2010, pp. 1198-1203.

[5] M. Arifujjaman, "Modeling, simulation and control of grid connected Permanent Magnet Generator (PMG)-based small wind energy conversion system," in *Proc. Electric Power and Energy Conference (EPEC), 2010 IEEE*, 2010, pp. 1-6.

[6] S. Breban, M. M. Radulescu, and B. Robyns, "Direct active and reactive power control of variable-speed doubly-fed induction generator on micro-hydro energy conversion system," in *Proc. Electrical Machines (ICEM), 2010 XIX International Conference on*, 2010, pp. 1-6.

[7] M. J. Khan, G. Bhuyan, M. T. Iqbal, and J. E. Quaicoe, "Hydrokinetic energy conversion systems and assessment of horizontal and vertical axis turbines for river and tidal applications: A technology status review," *Applied Energy*, vol. 86, pp. 1823-1835.

[8] V. J. Ginter and J. K. Pieper, "Robust Gain Scheduled Control of a Hydrokinetic Turbine," *Control Systems Technology, IEEE Transactions on*, vol. 19, pp. 805-817.

[9] V. J. Ginter and J. K. Pieper, "Robust Gain Scheduled Control of a Hydrokinetic Turbine Part 2: Testing," in *Proc. Electrical Power & Energy Conference (EPEC), 2009 IEEE*, 2009, pp. 1-5.

[10] W. E. Leithead, "Dependence of performance of variable speed wind turbines on the turbulence, dynamics and control," *Generation, Transmission and Distribution, IEE Proceedings C*, vol. 137, pp. 403-413.

[11] J. H. Laks and L. Y. Pao, "Optimal Control of Wind Energy Systems: Towards a Global Approach (Munteanu, I. et al.; 2008) [Bookshelf]," *Control Systems, IEEE*, vol. 29, pp. 105-108.

[12] W. E. Leithead, S. de la Salle, and D. Reardon, "Role and objectives of control for wind turbines," *Generation, Transmission and Distribution, IEE Proceedings C*, vol. 138, pp. 135-148.

[13] L. Kuo-Yuan, C. Yung-Ruei, and C. Yaw-Ming, "Battery charger with MPPT function for stand-alone wind turbines," in *Proc. Power Electronics Conference (IPEC), 2010 International*, 2010, pp. 932-937.

[14] M. J. Khan, M. T. Iqbal, and J. E. Quaicoe, "Effects of Efficiency Nonlinearity on the Overall Power Extraction: A Case Study of Hydrokinetic-Energy-Conversion Systems," *Energy Conversion, IEEE Transactions on*, vol. 26, pp. 911-922.

[15] A. M. De Broe, S. Drouilhet, and V. Gevorgian, "A peak power tracker for small wind turbines in battery charging applications," *Energy Conversion, IEEE Transactions on*, vol. 14, pp. 1630-1635.

[16] J. Khan, T. Iqbal, and J. Quaicoe, "Power tracking control challenges in Hydrokinetic energy conversion systems," in *Proc. Power and Energy Society General Meeting, 2011 IEEE*, 2011, pp. 1-6.

[17] T. Senjyu, R. Sakamoto, N. Urasaki, T. Funabashi, H. Fujita, and H. Sekine, "Output power leveling of wind turbine Generator for all operating regions by pitch angle control," *Energy Conversion, IEEE Transactions on*, vol. 21, pp. 467-475.

[18] R. Thresher, "A commercialization path and challenges for marine hydrokinetic renewable energy," in *Proc. Power and Energy Society General Meeting, 2011 IEEE*, 2011, pp. 1-8.

[19] http://pesn.com/2007/08/07/9500489_VAOT_v_HAOT/.

[20] L. Piegari and R. Rizzo, "A Control Technique for Doubly Fed Induction Generators to Solve Flicker Problems in Wind Power Generation," in *Proc. Power and Energy Conference, 2006. PECon '06. IEEE International*, 2006, pp. 19-23.

[21] X.-J. Yao, S. Liu, X.-D. Wang, C.-c. Guo, Z.-x. Xing, and H.-L. Jiang, "Doubly-fed induction generator control for variable-speed wind power generation system," in *Proc. Mechatronics and Automation, 2009. ICMA 2009. International Conference on*, 2009, pp. 855-859.

[22] P. Jungwoo, L. Kiwook, K. Dongwook, L. Kwangsoo, and P. Jinsoon, "An encoder-free grid synchronization method for a Doubly-fed Induction Generator," in *Proc. Power Electronics and Applications, 2007 European Conference on*, 2007, pp. 1-6.

[23] X. Weidong and W. G. Dunford, "A modified adaptive hill climbing MPPT method for photovoltaic power systems," in *Proc. Power Electronics Specialists Conference, 2004. PESC 04. 2004 IEEE 35th Annual*, 2004, vol. 3, pp. 1957-1963 Vol.3.

[24] J. Rizk and M. Nagrial, "Design of permanent-magnet generators for wind turbines," in *Proc. Power Electronics and Motion Control Conference, 2000. Proceedings. IPEMC 2000. The Third International*, 2000, vol. 1, pp. 208-212 vol.1.

[25] O. Keysan, A. S. McDonald, and M. Mueller, "A direct drive permanent magnet generator design for a tidal current turbine(SeaGen)," in *Proc. Electric Machines & Drives Conference (IEMDC), 2011 IEEE International*, 2011, pp. 224-229.

[26] J. F. Manwell, J. G. McGowan and A. L. Rogers, *Wind Energy Explained*: John Wiley & Sons, Inc., 2002.

VITA

Hailong Zhou was born on April 10, 1988 in Chengdu, Sichuan, China. He received his Bachelor of Science degree in Electrical Engineering from Chang'an University, Xi'an, China in June 2010. He started his Master of Science program in Electrical Engineering at Missouri University of Science and Technology in August 2010 and received his Master of Science degree in Electrical Engineering from Missouri University of Science and Technology in May 2012. His research interest includes hydrokinetic turbine systems and modeling, control and application of power electronic converters.